CHALMERS
UNIVERSITY OF TECHNOLOGY

Consequences on Ringhals Operation from Introduction of Adjacent Offshore Wind Power

Master's thesis in Electric Power Engineering

Mattias Fransson, Erik Johansson

DEPARTMENT OF ELECTRICAL ENGINEERING
CHALMERS UNIVERSITY OF TECHNOLOGY
Gothenburg, Sweden 2023
www.chalmers.se

Master's thesis 2023

Consequences on Ringhals Operation from Introduction of Adjacent Offshore Wind Power

Mattias Fransson, Erik Johansson

CHALMERS
UNIVERSITY OF TECHNOLOGY

Department of Electrical Engineering
Division of Electric Power Engineering
Chalmers University of Technology
Gothenburg, Sweden 2023

Consequences on Ringhals Operation from Introduction of Adjacent Offshore Wind Power
Mattias Fransson, Erik Johansson

Supervisors: Sofia Johansson, Magnus Knutsson, Mikael Nilsson, Ringhals AB
Examiner: Peiyuan Chen, Electrical Engineering

Master's Thesis 2023
Department of Electrical Engineering
Division of Electric Power Engineering
Chalmers University of Technology
SE-412 96 Gothenburg
Telephone +46 31 772 1000

Cover:400 kV transmission lines that connects Ringhals with the Nordic transmission grid. Typeset in LaTeX
Printed by TeknologTryck
Gothenburg, Sweden 2023

Consequences on Ringhals Operation from Introduction of Adjacent Offshore Wind Power

Mattias Fransson, Erik Johansson
Department of Electrical Engineering
Chalmers University of Technology

Abstract

As of the 16th of May, two offshore wind power plants (WPPs) located outside the coast of Halland was granted approval from the Swedish government. The combined installed capacity of the WPPs is expected to be over 1500 MW, and both prospectors were planning to connect to the same transmission lines that Ringhals power plant are utilizing, however when the approval came from the Swedish government only one of the projects were approved a large enough capacity to connect to the transmission grid. This has not been taken into account throughout the project so instead both WPPs are aggregated into a single power plant in this project. This report investigates possible electrical phenomena inherent to large scale WPPs that may affect the operation of a close by thermal power plant. A literature review was conducted which indicated subjects of interest, four key subjects were chosen to study further, namely harmonic emission, sub-synchronous oscillations, behavior during fault and abnormal grid states, and finally, inter-area oscillations. Through further literature analysis, the findings showed that harmonic emission should be manageable, while sub-synchronous oscillations could pose an issue given a situation of weakened grid and poor damping techniques. It was also found that there is a minor risk that an introduction of a WPP could increase the risk of inter-area oscillation. Dynamic phenomena was studied though extensive simulations in PSS/E, the simulations indicate that the grid, in its current condition should be able to sustain the impact of a sudden disconnection of a WPP without serious voltage deviations, and that the critical fault clearing times of the generators at Ringhals could either increase or decrease from an introduction of a WPP, depending on if the WPP rides through the fault or if it disconnects from the grid and if it injects any fault current or not. For cases were the WPP disconnects from the grid during fault the critical fault clearing time at Ringhals decreases noticeably whereas strong fault current injection from the WPP can increase the critical fault clearing times for the closest generator.

Keywords: Nuclear power plant, thermal power plant, wind power plant, wind farm, Type 4 wind turbine, sub-synchronous oscillations, inter-area oscillations, fault behavior, fault current injection, Ringhals.

Acknowledgements

We would like to express our deepest gratitude and appreciation to all the individuals who have contributed to the completion of this master's thesis. First, we would like to thank our supervisors Sofia Johansson, Magnus Knutsson and Mikael Nilsson for their support, guidance, and encouragement that have played a vital role in shaping this work. And our examiner, Peiyuan Chen, for exceptional mentorship, invaluable insights, and dedication throughout the research process.

We are grateful to Chalmers teachers and staff, particularly those in the department of electrical engineering, for giving us a supportive environment for studying and conducting research. The university's facilities, resources, and assistance were crucial to the effective completion of this thesis.

Finally, we would like to thank all the employees at Ringhals for having us, and for creating a welcoming and helpful atmosphere, for which we are incredibly grateful.

Mattias Fransson & Erik Johansson, Gothenburg, July, 2023

List of Acronyms

Below is the list of acronyms that have been used throughout this thesis listed in alphabetical order:

AVR	Automatic Voltage Regulator
CBG	Converter-based Generation
CFCT	Critical Fault Clearing Time
EAC	Equal Area Criterion
GUI	Graphical User Interface
IDE	Integrated Development Environment
IGBT	Insulated Gate Bipolar Transistor
LCC	Line Commutated Converter
NIMBY	Not in My Backyard
PCC	Point of Common Coupling
PMSG	Permanent Magnet Synchronous Generator
POD	Power Oscillation Damping
PSS	Power System Stabilizer
RfG	Requirements for Generators
RoCoF	Rate of Change of Frequency
SCC	Short Circuit Capacity
SG	Synchronous Generator
SSCI	Sub-synchronous Control Instability
SSO	Sub-synchronous Oscillations
SSR	Sub-synchronous Resonance
SSTI	Sub-synchronous Torsional Interaction
SvK	Svenska Kraftnät
TSO	Transmission System Operator
UIF	Unit Interference Factor
VSC	Voltage Source Converter
WECC	Western Electricity Coordinating Council
WPP	Wind Power Plant
WT	Wind Turbine

Nomenclature

Below is the nomenclature of parameters and variables that have been used throughout this thesis.

Parameters

UIF	Unit interference factor
MVA_{CNV}	Capacity of converter
MVA_{SG}	Capacity of synchronous generator
SC	Short circuit capacity at the converter station with the generator unit disconnected
SC_{TOT}	Short circuit capacity at the converter station with the generator unit in operation
SC_{G42}	Short circuit capacity contribution from G42
I_{max}	Max converter current
I_{qmax}	Max reactive converter current reference
I_{qmin}	Min reactive converter current reference
I_{pmax}	Max active converter current reference
I_{pmin}	Min active converter current reference
I_{Active}	Actual active current from WPP (in A)
$I_{ActiveP.U}$	Actual active current from WPP (in p.u)
$I_{Reactive}$	Actual reactive current from WPP (in A)
$I_{ReactiveP.U}$	Actual reactive current from WPP (in p.u)
Z_{Twind}	WPP step-up transformer impedance
Z_{line}	line impedance
Z_{T41}	Transformer 41 impedance
E	Back EMF
V_T	Terminal voltage
δ	Rotor angle

Variables

Kqv	Reactive current injection gain during over and low voltage conditions
Kvp	Voltage regulator proportional gain
Kvi	Voltage regulator integral gain

Contents

List of Figures

List of Tables

1

Introduction

In 2021 Sweden produced 165 TWh and consumed 140 TWh of electrical power [3]. Swedish electricity consumption has been stable since the nineties, but the consumption is predicted to increase drastically in the coming 20 years for several reasons [4]. Much of the increased electricity demand will come from the northern part of Sweden which is currently the part of Sweden that exports the most electricity. This will likely mean that the ability for the north to export to the south and other countries will decrease, so it is of vital importance that the southern parts of Sweden decrease their reliance on the north by increasing their own power production. A goal has been set in Sweden to only have renewable electricity production in the year 2040, so the possible power production types are limited to those that do not emit carbon dioxide while producing electricity [5]. For this reason, combined with geographical and technical reasons, the power production which is likely to increase most is wind power.

Producing electricity with wind power has become cheaper which has increased the interest of further expansion, although many wind power plant (WPP) projects are getting vetoed due to the "not in my backyard" (NIMBY) attitude of a large part of the population combined with local environmental concerns [6]. Therefore, building offshore WPPs is seen as a solution to this issue, since the WPP can be placed far enough out to sea so that the wind turbines (WTs) are not as visible. Building an offshore WPP also does have other benefits, such as higher average wind speed and more production hours throughout the year. Several offshore WPPs are in the planning phases in southern Sweden for these reasons.

Six nuclear reactors are producing power in the south of Sweden [7]. This generation is typically referred to as baseload power plants, which means that they operate at maximum capacity and are not regulated up or down to respond to changes in demand. The generators change their power factor to increase or decrease the amount of reactive power to the grid to keep the voltage stable. At this point it is not clear how these nuclear power plants would be affected from an electrical point of view if any or all the planned offshore WPP are built, e.g., if special phenomena inherent to a WPP interferes with electrical equipment or if significant changes in fault behavior could be experienced.

1.1 Plans for wind power plant

There are different companies planning WPPs in the sea close to Ringhals. One of these companies is Vattenfall and they have produced a report which describes in some detail what they are currently planning. Their report will be used as a basis for approximating theirs and the other WPPs characteristics in the later calculations and simulations [8], [9], [10].

The planned WPP will consist of Type 4 WTs, meaning that every WT has a dedicated converter that is dimensioned for the generators rated output. The output from these converters has a voltage of 66 kV. The cables from the WTs are then connected to a transformer station in the ocean which transforms the voltage from 66 to 400 kV. A 400 kV subsea AC cable is then laid on the ocean floor and connected to a connection point on land. Two of the projects are planning to connect on the Väröbacka peninsula, only a few kilometers away from Ringhals. From this connection point a new 400 kV line will be built, connecting to the existing 400 kV lines from Ringhals where the transmission lines are split up to bus A and bus B, as visualized in Figure 1.1 [8].

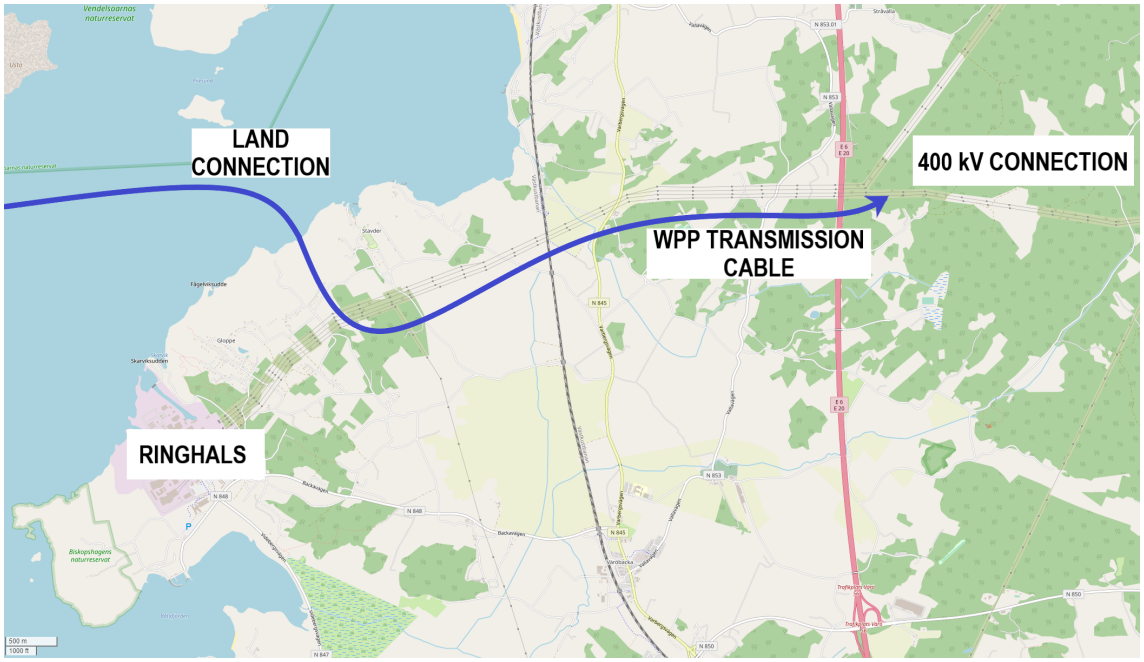

Figure 1.1: A map of the surrounding area with a likely cable corridor for the WPP from the sea to the 400 kV transmission grid.

As of the 16th of May, Vattenfalls project "Kattegatt syd" and part of OX2s project "Galene" have been granted approval the Swedish government [11]. The "Kattegatt syd" WPP has a planned installed capacity of 1200 MW and an annual production of 4.7 TWh, equivalent to approximately 3917 full load hours. The part of OX2s projects that has been approved, "Galene", is estimated to have an installed capacity of 415 MW and an annual production of around 1.6 TWh. Key information of the planned projects is listed below in Table 1.1.

Table 1.1: Estimated generation of planned Offshore WPPs outside the coast of Halland.

Project name	Connection	Capacity (MW)	Yearly generation (TWh)
Galene	Väröbacka	415	1.6
Kattegatt Syd	Väröbacka	1200	4.7
Stora Middelgrund	Breared	864	2.5-3.0
Kattegatt Offshore	Unknown	260	1
Total		2739	9.8-10.3

1.2 Aim

The aim of this thesis is to provide Ringhals AB with valuable information of phenomena that could affect onsite electrical and mechanical equipment caused by an adjacent connection of a large offshore WPP, both for steady state operation and dynamic events. The aim is also to provide general information which could be useful for other situations where a large thermal synchronous power plant is connected nearby to full power converter interfaced generation.

1.3 Project goals

The main goal of this project is to provide Ringhals AB with information on possible consequences and what needs to be prepared to interact with the offshore WPP in an efficient manner. This will be done through a literature review, where key finding will be more thoroughly investigated.

1.4 Scope

Integrating an offshore WPP into a power grid will have many different effects on the grid itself as well as the surrounding power generation. It is likely that this would result in the need for an expanded grid and other solutions, such as FACTS devices and energy storage. These types of changes to the grid will however not be part of this project and in the cases where the grid must be taken into consideration for simulations a simplified version of the equivalent circuit of the grid will be used.

Nuclear power plants are not used for frequency support in Sweden, thus the work will not explore whether or not it would be beneficial for Ringhals to change their power output in order to interact with the changing production profile of the WPP, hence if a generator at Ringhals is in use, it will operate at 100 % capacity.

Many different connection and production technologies may be chosen for the planned WPP. This project will assume the most likely alternatives, which is Type 4 WTs connected to the main grid through HVAC. Type 3 WTs will not be discussed and a

connection using HVDC will only be touched briefly. As the control mechanisms of WPPs are different for each plant, only general control mechanism will be investigated. Finally, issues that could occur between two WPPs will not be investigated. The planned WPPs will be investigated as one aggregated WPP.

1.5 Ethics

Ethics in the energy sector demand transparency and meaningful stakeholder engagement. The public has the right to be informed about the benefits, risks, and potential trade-offs associated with the integration of a nuclear power plant and a WPP. Ethical practices require open dialogue, accurate information dissemination, and opportunities for all stakeholder's participation. It is thus of vital importance that the result from this report is free from bias, so that conclusions drawn are true and does not minimize or exaggerate any of the risks or possibilities, to either act as proponents or opponents of the planned wind power expansion.

2
Theory

In this chapter, the basics of the theory needed to understand the report is presented. The theory focuses on the production methods of topic and its grid code requirements.

2.1 Ringhals power plant

Since the decommissioning of reactors R1 and R2, Ringhals power plant operates two active nuclear reactors, R3 and R4. Both are of pressurized water type and their planned lifespan runs into the 2040s. Each reactor powers two turbine generator sets. Each set has four turbines, one high pressure and three low pressure turbines all connected to the same shaft. The shaft is connected to the rotor of a turbogenerator with a rotating exciter. Each shaft is about 40 meters long and has many different natural frequencies that can cause oscillations in one part of the shaft. The synchronous generators (SGs) have a power rating of 677 MVA.

2.1.1 Automatic voltage regulator

The SGs are equipped with automatic voltage regulators (AVRs) which controls the generator terminal voltage. It does this by sending signals to the exciter of the SG, which increases or decreases the excitation which decides if the SG is over- or under excited, meaning if it is producing or consuming reactive power [12]. The AVR can be used with three different modes of operation, which are:

- Voltage control - The AVR operates to keep the voltage at the generator terminal constant by varying the excitation, the reactive power exchange will depend on the surrounding grid.

- Reactive power control - The AVR varies the excitation to keep reactive power export constant. In this case the voltage at the generators terminals will vary based on the surrounding grid.

- Power factor control - The AVR varies the excitation so that the power factor is kept constant, generator terminal voltage will vary based on the surrounding grid and reactive power exchange will only change when active power varies.

According to [13] Ringhals always operates all AVRs with voltage control.

2.1.2 Power system stabilizer

Another device called a power system stabilizer (PSS) is also connected to the AVR. According to [14] the damping of rotor oscillations is done through PSS. It dampens low frequency oscillations flowing in the power system by introducing a damping torque component, often by using the SGs speed deviation or active power as inputs. However, since the SG is frequency and phase dependent the PSS must also incorporate phase compensation to compensate for the lag between the output from the SGs exciter and the electrical torque. A PSS can be explained using three simple principles: a suitable gain, a high pass filter and lead lag filters. The gain makes sure that the damping is of the correct size, the high pass filter makes sure to remove the DC component of the signal, and the lead lag filters provide the phase compensation.

2.2 Offshore wind power production

This section describes the technical aspects of the proposed WPP and WTs according to [8], as not all elements are determined, some information will be taken from general guidelines and typical practices.

2.2.1 Wind power plant layout

A WPP consists of many WTs clustered together and interconnected through a collection grid, the proposed WPP "Kattegatt syd" is estimated to have between 60 and 80 WTs, with each WT having a power rating of 15-20 MW. The collection grid consists of numerous 66 kV cables, each with a transfer capacity of 80 MW. This means that each cable will interconnect four or five WTs. The cables are connected radially to a transformer station, where the voltage is transformed from 66 kV to 400 kV [8]. This means that from a grid point of view, the WPP will be seen as a single generating unit. A principal topology of a WPP is found in Figure 2.1.

2.2.2 Wind turbine topology

A Type 4 WT utilizes a generator connected to a full power converter. All current generated is processed by the converters, the generator is thereby isolated from the grid. This means that the specific dynamics and characteristics of the generator will not impact the grid. The full power converter is commonly composed of two voltage source converters (VSCs) that is converting the generated AC current to DC, then back again to AC [15]. Between the two VSCs a DC-link capacitor is connected which acts as a short time energy storage with the aim of keeping the DC-link voltage constant. Finally, a step-up transformer connects the VSC to the collection grid, transforming the voltage up to 66 kV [8]. A principal topology of a Type 4 WT is found in Figure 2.2.

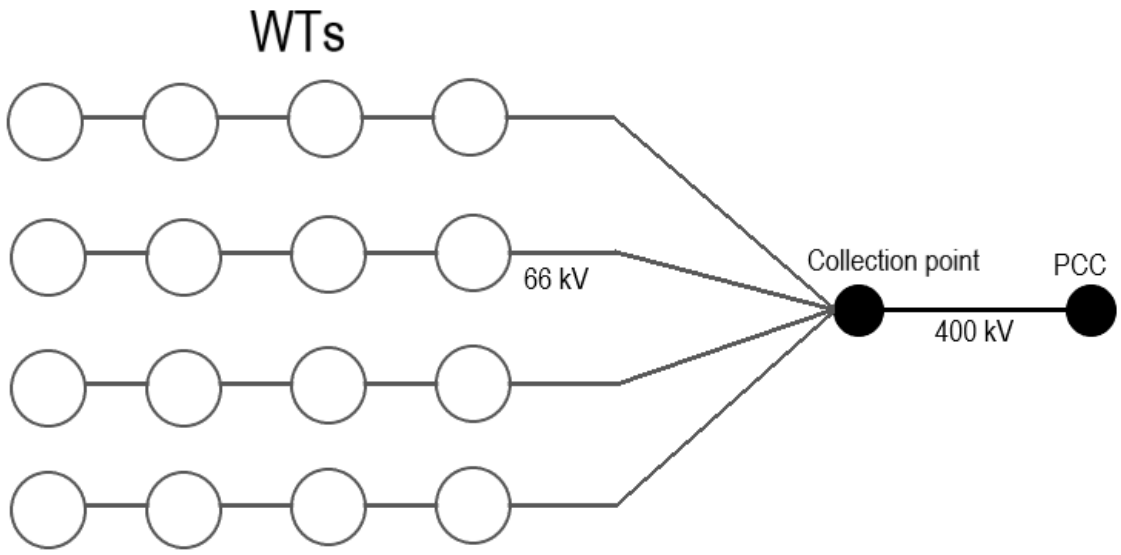

Figure 2.1: Generic WPP topology.

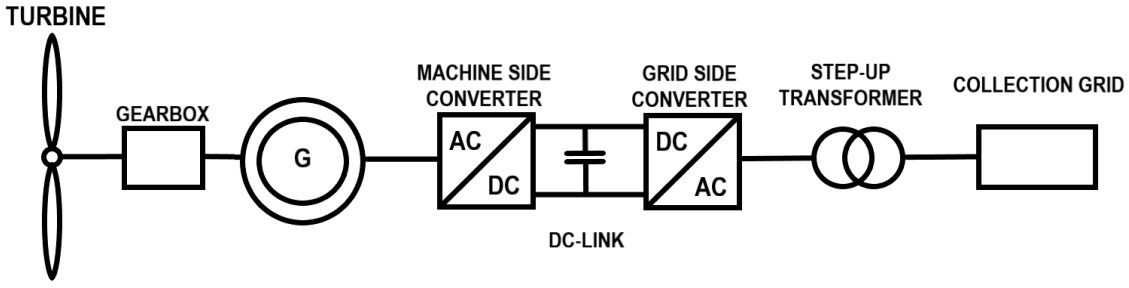

Figure 2.2: Generic Type 4 WT topology.

2.2.3 Voltage source converter

A VSC consists of forced commutated valves and can operate independently of the grid and is controlled with two degrees of freedom. For voltages up to 1800 V, the two-level VSC topology is commonly used. In this converter, each phase leg consists of two series connected semiconductor valves, for high power applications insulated gate bipolar transistors (IGBTs) are mostly used. The switching is most often controlled utilizing pulse-width modulation, with a switching frequency typically above 1000 Hz. For higher voltage applications the switching losses are higher, to cope with this the switching frequency is lowered, with the drawback that the harmonics generated from the switching are of lower order. Another way to manage the high losses is to use a multicell converter configuration, where multiple two-level VSCs are connected in parallel. Typically, this is used for power ratings higher than 3 MW and can thus be expected to be used for the proposed WPP. Although it cannot be said for certain which topology will be used, as there are many ongoing developments of high-power solutions for VSCs [16].

2.2.4 Wind turbine and plant control schemes

The grid side VSC mainly controls the DC-link voltage. Where the control system often consists of a fast inner current control loop which controls the current to the grid and a slower outer control loop that controls the DC-link voltage and the reactive power after the reference value received from the park controller. A phase-locked loop is used to estimate the grid voltage angle which the WT is synchronized to. The generator side VSC controls the generator current through an inner fast field-oriented current control loop and may also have a slower outer control loop that controls the flux and the torque of the generator [16].

The plant controller is the interface towards the grid and controls the active and reactive power delivered to the point of common coupling (PCC) according to set points for active and reactive power, voltage, or frequency. The reference values are then communicated to the individual WTs. The time constants for the plant controller are slower than that of the WTs, with a bandwidth below 50 Hz [16].

2.3 Grid codes

Grid codes are set for all power production methods connected to the public grid. These regulations cover both behavior during steady state and dynamic events. Different requirements are set depending on the production method, which in this report are synchronous production for Ringhals and power park modules for the WPP. Key aspects of the regulations for these production methods are found in this section.

2.3.1 Grid codes for synchronous production

Synchronous production units must obey a set of grid codes, one of the categories, fault ride-through, also known as low voltage ride through is defined as the ability of generators to stay connected to the grid during short periods of voltage levels below the systems rated voltage. For large production units like Ringhals certain regulations are set regarding fault ride-through [17]. There are general rules set by ENTSO-E in the document requirements for generators (RfG). In these rules, it is stated that the transmission system operators (TSOs) in Europe can create specific rules for production units connected to their grid.

A production unit of class D, which Ringhals is considered as, needs to be able to stay connected to the grid during a fault where the voltage in the connection point has the characteristics as seen in Figure 2.3, the voltage drops to zero for 0.2 seconds and when the fault is cleared the voltage immediately returns to 25% of the rated voltage. The voltage then increases so that it is back to 90% of rated voltage 0.75 seconds after the fault occurred. If the production unit has lost synchronism with the grid for a fault with this voltage characteristic at the connection point, the unit has not managed to ride through the fault.

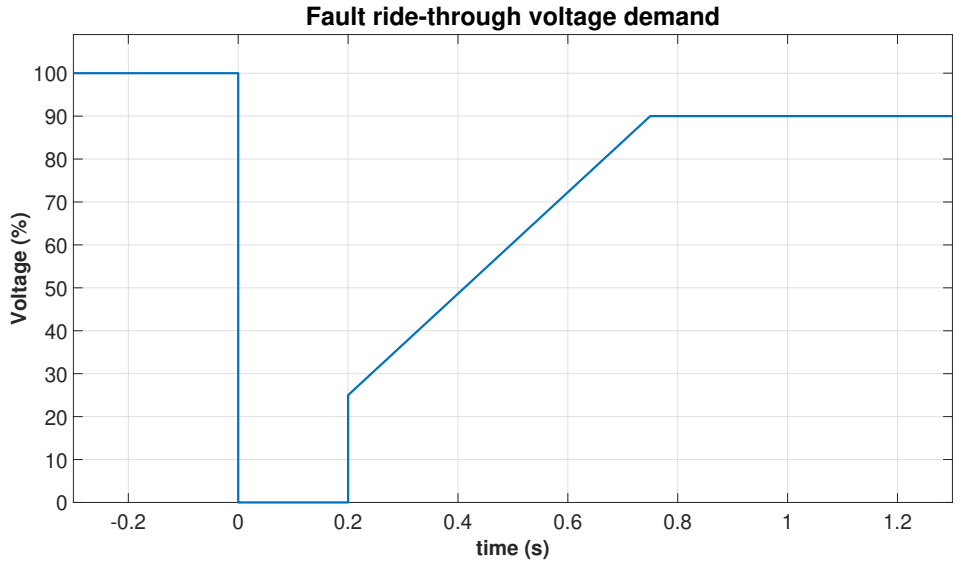

Figure 2.3: A graph showing the voltage drop that production units of class D needs to stay connected to the grid.

2.3.2 Grid codes for offshore wind power plant

Offshore WPPs have specific grid codes that the operator needs to ensure are followed. For reactive power support, the Swedish grid code states that an offshore WPP should be able to generate reactive power to the connection point equivalent to one third of the instantaneous active power production when operating in the interval of 90-102 % of nominal voltage. The same is applied to consumption of reactive power, but in the interval 95-105 %. The grid owner to the connection

point can however demand other requirements [18].

In [18] additional rules to RfG specifically for offshore power production are laid out.

Chapter 6, 1§ For offshore power park modules with a voltage between 300 and 400 kV in the PCC the modules must stay connected for 60 minutes for voltages between 105 and 110 % in the PCC.

Chapter 6, 2§ Offshore power park modules must have reactive power production capabilities that are equal to one third of the instantaneous active power in the voltage interval 90-102 % in PCC if the grid owners do not announce other demands.

Chapter 6, 3§ Offshore power park modules must have reactive power consumption capabilities that are equal to one third of the instantaneous active power in the voltage interval 90-105 % in PCC if the grid owners do not announce other demands.

Further, SvK have the authority to demand fault current injection from the WPP. Meaning that the WPP in case of a voltage dip will produce either active or reactive current to its capability with aim to keep the voltage to a higher level [19].

3
Methods

In this chapter, the main methods of the report, together with the key findings of the literature review will be explained. For certain chapters, the main method for finding useful information was through literature review, mainly in scientific article databases such as IEEE and Energiforsk. Calculations have been made using the equations originated from the scientific literature or textbooks within the area of electric power engineering. The results in chapter 6 and the short circuit capacities (SCCs) in chapter 5 was extracted from the power systems simulation software PSS/E.

3.1 Literature review

In the initial stages of this project attempts to reach out to nuclear operators with a WPP in their vicinity to learn from their experience were made. However, since nothing came of this, the main source of information was instead scientific articles. It should be noted that a lot of research in this area covers the topic of converter-based generation (CBG) as a replacement of synchronous production, the topic of addition of CBG is not as established, especially not within the topic of large production units electrically close to a large synchronous production unit. Hence, the literature review had a narrow search pool. The review can be divided into steady state and dynamic phenomena, such as disturbances. Below, a summary of issues identified from these articles is presented, some of which will be further studied in this report.

3.1.1 Identified phenomena

In [20] it is mentioned that due to the influence of the renewable energy sources, the stability in the grid has decreased and that harmonics caused by WPPs influences nearby SGs negatively with vibrations in the stator lamination.

Authors in [21] investigate a case study where sub-synchronous oscillations (SSO) between a Type 4 WPP and a thermal power plant occurred in China in 2015. The subjects are of key interest to Ringhals and was chosen to study further.

In [22] it is mentioned that a decrease in grid inertia due to higher renewable penetration will result in a less stable grid, which increases the risk for a large rate of change of frequency (RoCoF) during faults or imbalances in said grid. This was not

investigated further since what was being considered in this report was not replacing synchronous generation with CBG, only the addition. Effects that are likely to occur in the case of replacement was only covered briefly as a part of chapters where it became necessary. Furthermore, the focus of this report lies in the local impact.

In [23] it was found that for certain weak grids the fault current injection from WPPs can make a significant difference during faults in the system, both for frequency and voltage. By retaining the active power from a WPP during a fault through current injection, the active power recovery of the WPP was seen quicker, thus achieving a higher frequency nadir. Although as mentioned in the previous paragraph, frequency deviations are closely linked to grid inertia and the addition of a WPP will not decrease grid inertia unless it is replacing traditional generation, so frequency deviations fall outside the scope of this project. Voltage levels are however very local, so a study with the aim of measuring how a fault current injection from the WPP will impact the system voltage was undertaken. Because of the potential for higher retained voltages during faults, the critical fault clearing time (CFCT) of the Ringhals generators was also deemed an interesting area of study.

Authors in [13] investigates the reactive power resources in the surrounding grid of Ringhals after the decommissioning of R1 and R2. It showed that Ringhals reactive power resources had at times been utilized to a high degree unnecessarily. Poor reactive power management from grid operator had resulted in situations where Ringhals had produced a high amount of reactive power while at the same time consuming the reactive power through shunt reactors at connecting buses. A large WPP could potentially help in this regard, but it might also complicate the reactive power coordination in the grid. It also raised questions of how severe of a voltage drop or increase could be if the WPP takes on a leading role of reactive power supply to the grid and is then suddenly disconnected, especially if one of the reactors at Ringhals is disconnected due to maintenance. To study this, simulations were made when the WPP was tripped during different load situations.

Inter-area oscillations can cause problems such as sub-optimal power flows and inefficient operation for power systems. Authors in [24] attempt to study how increasing wind integration in Norway impacts the two well-known inter-area modes in the Nordic grid. The authors find that Type 4 WTs decrease the damping of the modes. The article is quite old, so the Type 4 WTs are modeled simply as negative loads which amplifies oscillations when they occur. The article also mention the fact that the WTs can probably be equipped with stabilizing controllers. It is therefore important to try and find more recent information about how or if a Type 4 WPP interacts with inter-area modes and if this interaction is likely to have a negative impact on Ringhals.

To summarize, four subjects of interest will be studied further in this report, namely harmonic emissions, SSO, behavior during fault and abnormal grid states, and finally inter-area oscillations.

3.2 Simulations in PSS/E

PSS/E or "Power System Simulator for Engineering" is a widely used program that was first introduced by Siemens in 1976. It is used by many different companies within electric power engineering and is a commonly used tool for TSOs as well. In the program, the single-line diagram of power systems is modeled, parameters are set, and different load flows can be evaluated on the system. After a specific load flow is set, it is possible to run dynamic simulations in the program to observe the behavior of the system during different faults.

A problem with running the simulations like this is that it takes a long time to initialize new simulations and run them in PSS/E. If the network is large, there is a risk that the program may crash before yielding any useful results. A powerful solution to these problems is to run PSS/E through a Python Integrated Development Environment (IDE).

3.2.1 Running PSS/E through Python

Python is an object-oriented programming language with a dedicated package for running PSS/E. It enables simulations using PSS/E without the use of the graphical user interface (GUI). Instead, PSS/E can be run through an IDE. An IDE is a program used for writing, running, and debugging code. For this project, the IDE PyCharm has been used but there are many other IDEs with similar functionality. The code can be written from scratch in the IDE, but PSS/E also has a function that lets the user record their work inside the GUI and then export the actions the user has taken in the GUI into a Python file to enable repeatability more conveniently. The graphing of data in PSS/E is quite limited so it is also useful to use a command in Python that converts the output file into another file type, for example, .txt, which can be read by another program, such as MATLAB which was used for plotting in this case.

3.2.2 Simulation of maximum fault currents

The maximum fault currents was acquired though PSS/E, using the function "SCMU", which calculates instantaneous fault currents based on the subtransient impedances of the generators.

4

Harmonic Emission

Recent developments, related to WPPs, have made the issue of harmonic emission more complicated. Emission shifts to higher frequencies, where impedance models are less developed. At the same time, resonances shift to lower frequencies, so that even for lower frequencies impedance estimates become less accurate [25].

Analysis of harmonic distortion at the PCC not only requires an adequate WT harmonic model but also an appropriate harmonic propagation study methodology when there are multiple WTs interconnected. Hence, this chapter will only cover a prediction of harmonic emissions from a WPP under normal operation in the surrounding grid, based on typical characteristics of WTs.

4.1 Harmonic regulations

Harmonics are sinusoidal voltages or currents with frequencies that are integer multiples of the fundamental frequency, with a non-integer multiple of the fundamental frequency they are referred to as inter-harmonics. Harmonics flowing in an electrical circuit distort the fundamental waveform and can cause damage or premature deterioration of electrical equipment, thus, regulation of harmonic emissions is set. In Table 4.1 IEEE Std 519-2014 recommendation of maximum current harmonic emissions from a production unit at voltages higher than 161 kV is found [1].

Table 4.1: Maximum harmonic current distortion in percent of I_L as per IEEE Std 519-2014 [1].

Harmonic order (h)	**Relative current (I_L)**
3-10	1.0 %
11-16	0.5 %
17-22	0.38 %
23-34	0.15 %
35-50	0.1 %
THD	1.5 %

For even harmonics, 25 % of the values above is the limit. I_L is the maximum demand load current at the PCC under normal load operating conditions, i.e., when both the WPP and Ringhals are operating at maximum capacity. The above values are valid when the maximum short-circuit current at the PCC, I_{SC}, divided by I_L

is under 25. With the WPP and Ringhals operating at maximum, the production is around 2000 MW, I_{SC}/I_L would be roughly equal to 10, with I_L equal to 2.89 kA and I_{SC} around 29 kA.

In the European standard "EN 50160:2010" harmonic distortion limit is given for voltage harmonics relative to nominal voltage, u_h, these are found in Table 4.2 below. Notable is that in case of complaints, the limits could be lowered in concurrence with the TSO [2].

Table 4.2: Voltage harmonic limits as per EN 50160:201 [2].

Odd harmonics				**Even harmonics**	
Nonmultiple of 3		**Multiple of 3**			
Order (h)	Relative voltage (u_h)	Order (h)	Relative voltage (u_h)	Order (h)	Relative voltage (u_h)
5	5 %	3	3 %	2	1.9 %
7	4 %	9	1.3 %	4	1 %
11	3 %	15	0.5 %	6...24	0.5 %
13	2.5 %	21	0.5 %		
17	-				
19	-				
23	-				
25	-				

It is important to keep in mind that when measuring harmonics, it is not possible to distinguish between the primary and secondary emission, i.e., the emission owing to the intended source of measurement and the emissions owing to the grid [25].

4.2 Harmonic emission from Type 4 wind turbine

The source of harmonic emission from a Type 4 WT is mainly dependent on its power electronic converters. As opposed to, for example, a WT with a generator directly connected to the grid. This is due to the full conversion of the current coming from the generator. The harmonic content from a Type 4 WT can be divided and categorized as characteristic harmonics and non-characteristic harmonics. Characteristic harmonics are generated from the pulse-width modulation of the converter, the main characteristic harmonics from a Type 4 WT will occur around multiples of the switching frequency. Given a typical switching frequency in the region of 1-2 kHz, the first main characteristic harmonic would be found around the order between 20 and 40 if the fundamental frequency is 50 Hz. The switching frequency is normally set as a multiple of three of the fundamental frequency. The largest harmonic component would thus result in a zero-sequence harmonic that cannot travel through the transformer of the WPP, if it is composed of a delta winding [26], [27]. Non-characteristic harmonics are those that are generated due to non-ideal conditions, implementations, operating point, and control scenario of the individual converter and is thus not related to the converter topology, these harmonics are

typically lower order compared to the characteristic harmonics [27], [28].

Generally, grid compliance on harmonic limits is manageable for a single WT, however, when multiple WTs are interconnected it is not a trivial issue. Authors in [27] states that the characteristic harmonics from different WTs in a WPP are at random phase and does not act in unison, due to each converter operating with a slightly different switching frequency. The summation of the harmonics from the different WTs at the PCC is thus random, and some may cancel each other out. However, [26] suggests that there is a considerable risk that harmonics from different sources superposition, resulting in harmonics with significant amplitude. Authors in [28] mentions that characteristic harmonics do show a certain degree of correlation among the different WTs, determined by the modulation technique. For non-characteristic harmonics it is suggested that the correlation is low or even completely uncorrelated between different WTs.

Authors in [25] suggests using an aggregation factor to estimate the harmonic levels at the PCC, defined as the emissions into the grid divided by the total emissions from the individual WTs. An estimate of the aggregation factor is one divided by the square root of the number of WTs. Although it is stated that this is often a too simple approximation, as it does not consider any resonance phenomena within the WPP.

4.3 Harmonic resonance & aggregation

Due to inductance and capacitance present in the collection grid of a WPP, resonances occur that increases or decreases the harmonic emission into the public grid [29]. The resonance typical of a WPP can be characterized by either series resonance or parallel resonance. Parallel resonance occurs when the equivalent impedance of the WPP can be simplified to a capacitor and an inductor in parallel. Specific for this is that when analyzing the equivalent impedance of the system at a certain point, there is a remarkably high value at a specific frequency. This characteristic may cause current harmonics injected nearby to produce high voltage distortions. When the equivalent impedance instead can be simplified as a capacitor and an inductor in series, series resonance occurs and results in a low impedance at a certain point and at a certain frequency. This may result in high current distortions when voltage harmonics are injected, e.g., from the WTs, [26]. Series resonance is most dominant in a typical offshore WPP.

In [30] harmonic emission measurements are presented for a WPP composed of ten WTs. The result compares the emissions from individual WTs and the plant. Here it is found that harmonics well below the resonance point (1550 Hz), in the region of 100-350 Hz, have an aggregation factor of about one, meaning that the harmonics from the individual WTs can be summed up to get the harmonic emission into the public grid. Interharmonics in this region is dampened with the square root of ten, as suggested earlier. Both harmonics and interharmonics around the resonance

frequency (1550 Hz) are amplified with up to six times. For harmonics above the resonance frequency the amplitude is further damped.

The findings in [30] resemble those of, for example, [29] and [25]. Common for these sources is that the WPP studied consists of fewer and smaller WTs than what is currently planned in this case. With more WTs the result may look different. Although if the same principle is used as in the sources mentioned, low-order harmonics will have close to linear addition while interharmonics and harmonics above the resonance frequency can be assumed to aggregate with random phase angle, meaning aggregation with one divided with the square root of number of WTs. From these sources, it can also be seen that in relative terms, the amplitude of low order current harmonics are a few times higher than the harmonics around the resonance frequency. The actual amplitude of the harmonics that will be produced from the planned WPP is difficult to estimate, as it depends heavily on the components used and to which degree filtering and damping are implemented. Authors in [27] concludes that the amplitude of low order harmonics at the PCC are comparable to that of a SG, around 1 %.

4.4 Conclusion

From the findings in this chapter, it can be concluded that the harmonics injected into the public grid adjacent to Ringhals from the WPP are likely to have the following characteristics:

- Current harmonics are dominant.
- Low order harmonics equivalent to that of an equally sized SG (in combined WT generation capacity).
- High order harmonics around the switching and resonance frequency, likely in the region of 1-2 kHz, with amplitude lower than that of the low order harmonics.
- Inter-harmonics and high order harmonics will aggregate with a one divided by the square root of the number of WTs.
- Supraharmonics well above the main resonance frequency will be heavily dampened and should not be of concern.

Further, is is of importance to Ringhals to minimize harmonic emission in the connecting grid, as it can cause damage or premature deterioration of electrical equipment.

5
Sub-Synchronous Oscillations

With the latest rapid increase of CBG a new concern has arisen regarding adverse interactions between different power system elements resulting in unstable behavior of the system. One of which, SSO could pose a serious threat to the power system given certain circumstances. In this chapter, a brief introduction to SSO is given, together with information on what causes the phenomenon and how to mitigate it. An indication of the risk of SSO caused by a WPP installation adjacent to Ringhals is also discussed.

5.1 Definitions

Many different definitions and categorizations can be found in the subject of SSO. The traditional definitions were defined for sub-synchronous stability issues related to conventional turbogenerators, since the introduction of complex CBG, such as Type 3 and 4 WTs, the definitions have been changed. In this report, ENTSO-Es definitions from 2018 will be used [31], which are the basis of the definitions listed in this section.

5.1.1 Sub-synchronous oscillation

SSO is a collective term for electro-mechanical interactions below fundamental frequency, either between a turbine-generator and passive system elements, or between a turbine-generator and active system elements, such as HVDC transmission system equipment control and static VAR system controls [31]. If SSO is present near a turbine-generator set mechanical oscillations could occur, which, depending on severity, may cause fatigue, damage to shaft, or triggering of protection equipment [16]. The three different categories of SSO listed in this report differentiates mainly by its origin and the affected instrument, as per Figure 5.1.

5.1.2 Sub-synchronous resonance

Sub-synchronous resonance (SSR) is the interaction between mechanical/torsional masses in a generator and the electrical resonance from series compensation (capacitor) [31]. SSR is the traditionally studied SSO phenomenon and can further be divided into transient SSR and steady state SSR [16].

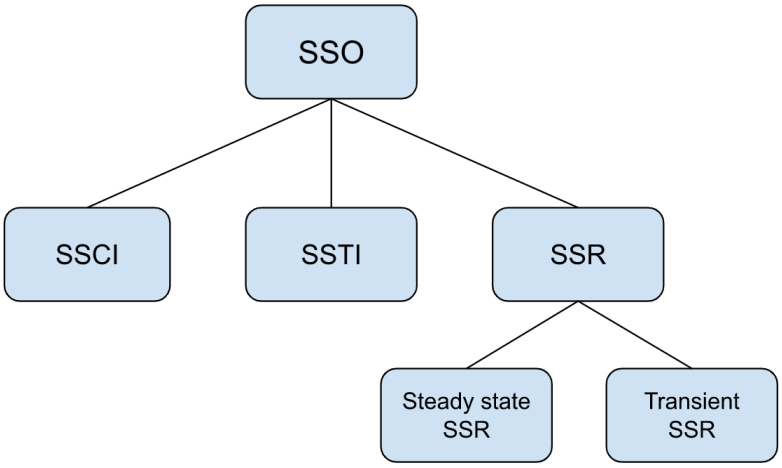

Figure 5.1: SSO hierarchy. The three types of SSO differentiates mainly by its origin and the affected instrument.

5.1.3 Sub-synchronous control instability

Sub-synchronous control instability (SSCI) occurs when there is an exchange of energy between the power electronic converter controllers and the series compensation capacitor of the transmission lines due to the interaction between the control system of converters and the series capacitor. This problem is most common for Type 3 WTs, Type 4 WTs are known to be immune to SSCI, due to the full power conversion from the generator [32].

5.1.4 Sub-synchronous torsional interaction

Sub-synchronous torsional interaction (SSTI) is the dynamic interaction between the mechanical/torsional masses in a generator and a power electronic device, such as an HVDC link, static VAR compensator, or WT [31]. This is the type of SSO that will be of concern to Ringhals regarding the proposed WPP and will further be discussed in the sections below.

5.1.5 Unit interference factor

A unit interference factor (UIF) is a screening level indicator of the risk of torsional interaction between a generating unit or power plant and an HVDC converter, it can be calculated as

$$UIF = \frac{MVA_{CNV}}{MVA_{SG}} \left(1 - \frac{SC}{SC_{TOT}}\right)^2 \tag{5.1}$$

Where MVA_{CNV} is the capacity of the converter, MVA_{SG} is the capacity of the SG, SC is the short circuit capacity (SCC) at the converter station with the generator unit disconnected and SC_{TOT} is the SCC at the converter station with the generator

unit in operation [16], [33]. UIF should be calculated for carefully selected (credible) N-x outage conditions [34]. It is also important to consider that the interaction between the WPP and Ringhals should be analyzed not only for the existing grid, but also for any changes in the grid that will take place in the lifetime of the WPP or Ringhals lifetime [31].

If the UIF of the studied generator is greater than 0.1 further studies of SSO is recommended. A UIF less than 0.1 should not have significant interaction with the converter and could be neglected for further studies [16], [33]. However, the guideline of 0.1 is verified with line commutated converters (LCC) and not VSC as used in [16], where it was found that an UIF of 0.079 gave an increased risk of SSO, and thus it was recommended to lower the guideline of 0.1 for VSC. In [35] it is stated that generators with UIFs around 0.05 could be prone to SSO.

5.2 Causes & risk amplifications

SSO between a steam turbine-generator and a Type 4 WPP are rare and with proper design choices and mitigation techniques the issue should not occur. Although the phenomena has been observed in some cases and it should be noted that as of now there are very few examples where a large Type 4 WPP has been closely connected to a large steam turbine-generator, as up until recently, WPPs of the proposed magnitude have mostly been comprised of Type 3 WTs.

5.2.1 Causes

The torsional system of a turbine-generator set has a positive mechanical damping, while a VSC or a group of VSCs could cause a negative electrical damping at some frequencies. If the overall damping of the electrical system is low or negative at the torsional mode frequencies of the generator shaft a Type 4 WPP could cause SSO. The bandwidth in which SSO could occur is commonly 10-30 Hz, here typically lies the torsional mode frequencies of large steam turbine-generators and is also the bandwidth that some control schemes of the WPP uses [16], [35]. For a WPP, both the control of the park and the individual WTs risk contributing to SSO. The control schemes vary between different WPPs, although, in the WTs it is the phase-locked loop that has a bandwidth below 50 Hz. For the park control it is normally the part that controls active and reactive power that has a bandwidth below 50 Hz [16].

5.2.2 Risk factors

There are a few key elements that impact the risk of SSO. From equation 5.1 of the UIF, it can be seen that there are three factors that impact the risk of SSO, the MVA rating of the WPP and the SG, the grid strength, i.e., the SCC at the connection point of the WPP and finally the relation of the SCC with and without the SG. The relation of the SSC is an indication of the electrical distance between

the SG and the WPP.

Although, there are more factors that will determine the risk, in [16] and [21] simulations of the change of electrical damping were conducted when several factors were altered. In [16] it was concluded that a high gain of the AC voltage controller, low grid strength and a small electrical distance between the WPP and the SG indicated an increased risk of SSO. A similar conclusion was found regarding grid strength in [21]. In the same study, the effects of the number of online WTs were also studied, where it was found that the damping and the frequency of SSO have a negative correlation with the number of online WTs. Lastly, the WT grid side converter controller parameters were studied, and the result showed that some of the parameters had a positive correlation with the damping and some had a negative correlation.

In summary, the risk of SSO between a Type 4 WPP and a turbine-generator set is mainly determined by grid strength, electrical distance to the turbine-generator, size, and operating point of WPP, strength and parameters of WPP and WT controllers, and finally the characteristics of the turbine-generator set.

5.3 Risk assessment

When calculating the UIF, the SCC has been calculated at the 66 kV wind bus, closest to the WPP in Figure 5.2, through PSS/E with saturated subtransient impedances for the Ringhals generators, results with unsaturated impedances can be found in appendix A. For the calculations, a second transformer was added between the WPP and the 66 kV bus, with a 1:1 ratio, 1500 MVA rating and a reactance of 0.1 p.u. This transformer represents an aggregation of the transformers at the individual WTs. The result is found in Table 5.1 and 5.2 for G32 and G42 respectively, where the SCC and UIFs are found for the different models and with different grid strengths, calculated with equation 5.1. The models "Standard", "Parallel", and "Own line" are found in Figures 6.1, 6.2, and 6.3 respectively. The highest grid strength represents the case where all Ringhals generators are online, and all transmission lines are in use. In Figure 5.2 the grid representing the lowest grid strength is shown, here only the investigated Ringhals generator is online, the transformer between the swing bus and bus B is also out of service. The feasibility of this scenario is discussed later in this section.

No clear statements have been found if the SCC contribution from the WPP should or should not be used in the calculation of UIF. Although it seems that in [16] it is not used, and considering that there is no demand of fault current injection it is a possible scenario that the WPP would not provide any short circuit power, therefore, the contribution from WPP is not included in the calculation. This will also give a higher UIF, hence a conservative scenario. The capacity of the converter was set to 1500 MVA, and the capacity of the SG to 677 MVA. If the WPP would be included in the fault current contribution, and a fault current injection of 1.2 p.u was to be used, the SCC at the WPP bus would increase with up to 1800 MVA.

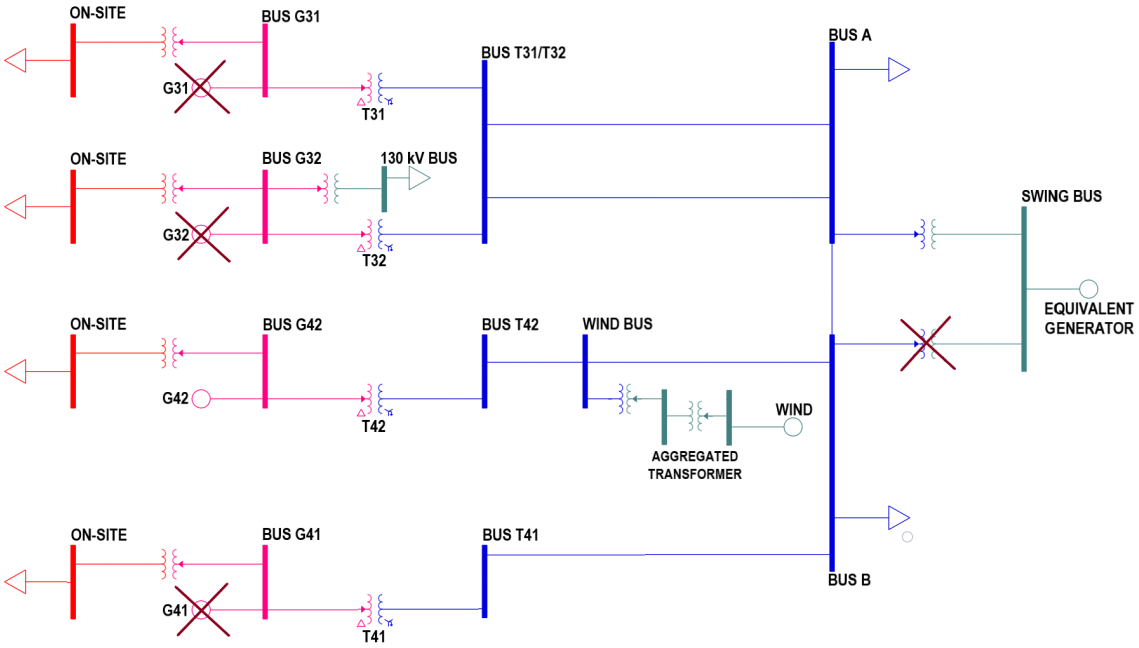

Figure 5.2: Representation of weak grid.

Table 5.1: UIF for G32 and SCC at the bus closest to the WPP for different models and grid strengths.

Model	Grid strength	SC_{TOT} (MVA)	SC (MVA)	UIF
Standard	High	4205	4153	0.0003
Standard	Low	2654	2404	0.0198
Parallel	High	4570	4501	0.0005
Parallel	Low	2746	2446	0.0264
Own line	High	3685	3629	0.0005
Own line	Low	2426	2167	0.0252

Table 5.2: UIF for G42 and SCC at the bus closest to the WPP for different models and grid strengths.

Model	Grid strength	SC_{TOT} (MVA)	SC (MVA)	UIF
Standard	High	4205	3952	0.0080
Standard	Low	2958	2404	0.0777
Parallel	High	4570	4382	0.0038
Parallel	Low	2970	2446	0.0690
Own line	High	3685	3611	0.0009
Own line	Low	2526	2167	0.0447

If the WPP would be connected to the transmission grid using HVDC, the origin of SSO could lie in the controls of the HVDC controller, in this case no aggregated transformer should be used for the calculations. The results for the UIF of G32 and G42 with this case can be found below in Table 5.3 and 5.4 respectively.

Table 5.3: UIF for G32 and SCC at the bus closest to the WPP for different models and grid strengths, in the case of HVDC connection.

Model	Grid strength	$\mathbf{SC_{TOT}}$ (MVA)	SC (MVA)	UIF
Standard	High	5804	5706	0.0006
Standard	Low	3174	2796	0.0314
Parallel	High	6547	6428	0.0007
Parallel	Low	3425	3010	0.0326
Own line	High	4859	4777	0.0006
Own line	Low	2938	2604	0.0286

Table 5.4: UIF for G42 and SCC at the bus closest to the WPP for different models and grid strengths, in the case of HVDC connection.

Model	Grid strength	$\mathbf{SC_{TOT}}$ (MVA)	SC (MVA)	UIF
Standard	High	5804	5337	0.0144
Standard	Low	3617	2796	0.1142
Parallel	High	6547	6195	0.0064
Parallel	Low	3779	3010	0.0917
Own line	High	4859	4746	0.0012
Own line	Low	3077	2604	0.0524

If Table 5.3 and 5.4 are compared to Table 5.1 and 5.2, it can be seen that the UIF is higher for the case of HVDC. The reason for this is the increased difference in SCC when the investigated generator is connected and disconnected. The reason for the increased difference is due to the absence of the aggregated transformer. The SCC for the case of HVDC was acquired at the 66 kV wind bus, found in Figure 6.1. The 66 kV side was chosen as a grid side transformer is typically used after a HVDC-converter, the 400 kV transformer in the model was used to represent this. No HVDC-controller was modeled, as there is no need for it when calculating the UIF.

To see how much the UIF for G42 may change with the SCC for the "Standard" model, a plot is shown in Figure 5.3. As can be seen in Table 5.2, the difference between SC_{TOT} and SC i.e., the SCC contribution from G42, SC_{G42}, varies depending on grid strength. The value of SC_{G42} was taken for a few samples in the grid strength region between 2200 MVA to 4300 MVA, and found to vary within this region with the equation

$$SC_{G42} = \frac{2650000}{SC_{TOT}} - 375 \tag{5.2}$$

This equation is only an estimate and valid for the region 2200 MVA to 4300 MVA. The equation used for the plot is

$$UIF = \frac{1500}{677}\left(1 - \frac{SC_{TOT} - SC_{G42}}{SC_{TOT}}\right)^2 \tag{5.3}$$

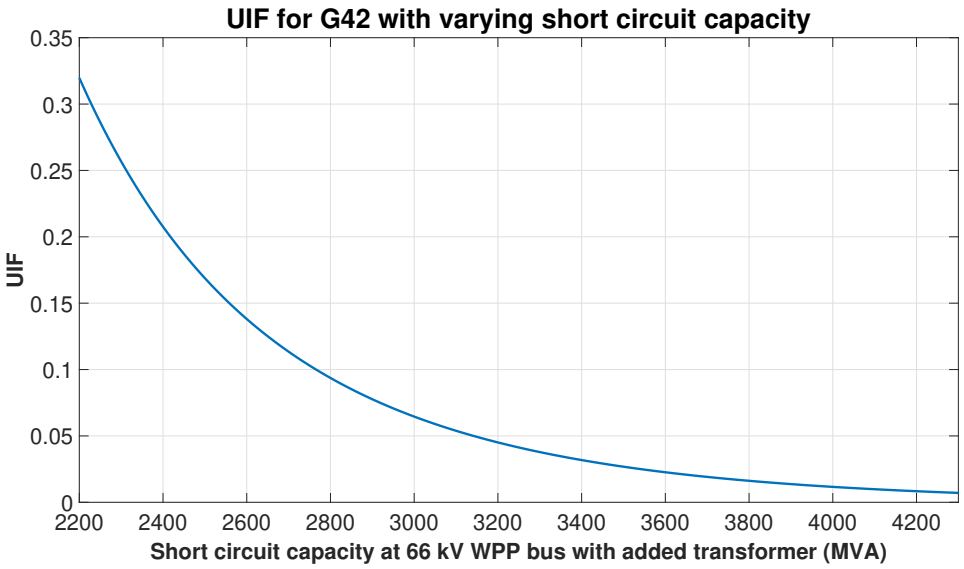

Figure 5.3: UIF with varying SCC.

A UIF of 0.05, as stated in [35] could be prone to SSO, if the SCC is around 3142 MVA. This is not unreasonably low, considering a future scenario where synchronous production has been replaced with CBG and/or a transmission line bus B is out of service. The lowest reasonable SCC was also be estimated from the SvK model, but the result is not listed in this report due to company confidential information.

5.4 Other cases and risk mitigation

As previously mentioned, few cases of SSO caused by Type 4 WPPs have been documented. The first reported case occurred in China in 2015, where at one instance, oscillations originated from a Type 4 WPP stimulated intense torsional vibration in nearby turbogenerators, resulting in the trip of all the generators in a power plant by its torsional protection system. The frequency of the oscillations during the whole event varied in a range from 27 Hz to 33 Hz. The power system in the effected area has similarities to the surrounding grid of Ringhals. No series compensation is located nearby, both the power plant effected and the WPP are of comparable size and the WPP is connected through AC. The SCC at the WPP causing the SSO is however lower, on the other hand, the electrical distance to the power plant seems to be larger [21].

Mitigation of SSO is standard for an HVDC-system, but due to different requirements, it is not standard for WPPs. If the WPP is suspected of being able to cause issues of SSO mitigation techniques can be implemented. Although as previously mentioned, both the WT controller and WPP controller could contribute to SSO, which makes SSO mitigation more complex compared to an HVDC converter, where a sub-synchronous damping controller is commonly used if needed [16]. While no clear rules have been found of mitigation requirements, it should lie in all stakeholder's interest to minimize the risk.

There is no rich literature about SSO damping methods in Type 4 based WPPs, although there is no general method, there are some proposed methods, found in e.g., [16] and [36] which are presented below. The most basic technique is to optimize the control parameters of the grid side converter of the WTs, with the aim of reshaping the equivalent impedance characteristics of the WTs, to provide positive electrical damping around critical frequencies. Another method is to let the grid side converter be used to provide additional SSO damping. The proposed method utilizes an active damping impedance control, to reshape the impedance property of grid side converter. Finally, it is suggested that a supplementary STATCOM device can be used to dampen SSO when operating in reactive power control.

5.5 Discussion & conclusions

From Table 5.1 and 5.2 it can be found that the different connection alternatives result in a significant difference in UIF for G42, but not for G32. Overall, the results indicate insignificant risk for SSO at all models and grid strength for G32. For G42 there is a moderate risk that SSO could occur at low grid strength, especially for the model's "Standard" and "Parallel". The equation for UIF takes on few parameters, hence, the only reason for the lower values is the difference in SCC. The difference in relation of the SCC signifies both the electrical distance between the WPP and the generator-turbine set and the grid strength. The resulting UIF is largely dependent on the SCC, as seen in Figure 5.3, hence notes the importance of choosing a correct N-x outage. It is also of importance to estimate if a notably lower SCC could be expected at the end of either Ringhals or the WPP lifespan.

As described in section 2.2, each WT has its own transformer, therefore the most realistic representation of the WPP, in regards to the SCC calculated for the UIF, was determined to be with the addition of a second transformer on the 66 kV side to represent an aggregation of the WTs transformers, this had also been done in [16]. As previously mentioned, it is both the WT and the park controller that could cause SSO, with this, one could conclude that the aggregated transformer is incorrect regarding SSO caused by the park controller, as this is located outside the WTs. Although the understanding is that it is the resultant output from the WTs, influenced by the controllers, that is the root cause of SSO.

As stated in [16], it is not yet established what the guideline for a possible lowest UIF should be regarding a large SG and a VSC or WPP, and as numerous results are not too far off the reference of 0.079, further SSO studies are necessary. Finally, the effectiveness of mitigation approaches is hard to estimate, and the only results found are of simulations, not real-life measurements. Reasonable, the mitigation methods should only be necessary to counteract the interactions with Ringhals, as other power plants are located much further away.

6

Behavior During Fault and Abnormal Grid States

In recent years, TSOs around the world have put new requirements in place that demand large reactive power capabilities from WPPs, this could lead to a situation where the new WPP close to Ringhals is producing large amounts of reactive power, so that less reactive power resources from Ringhals are needed. As mentioned in chapter 2, SvK in conjunction with other relevant grid owners can demand active or reactive current injection during grid fault conditions from the WPP [19]. Since it is not clear yet what the requirements are going to be, a few different variations will be studied in this chapter. Furthermore, this chapter will also cover how a WPP will affect the CFCT of Ringhals, the impact of a sudden trip of the WPP and differences in maximum fault currents.

6.1 Possible grid connections of wind power plant

To simulate transient phenomena like a fault on one of the 400 kV buses close to Ringhals or a loss of production from the WPP a model resembling Ringhals and the surrounding grid is needed. For this purpose, a PowerFactory model used in an internal Ringhals report has been adapted into PSS/E, the single-line diagram of the model is shown in Figure 6.1 and is named "Standard". The model is based on the electrical configuration at Ringhals after the decommissioning of R1 and R2. Before the decommissioning, each reactor had one dedicated 400 kV line but after the shutdowns, a large project was undertaken at Ringhals so that R3 will feed the two lines going to bus A and R4 will be connected to the lines going to bus B.

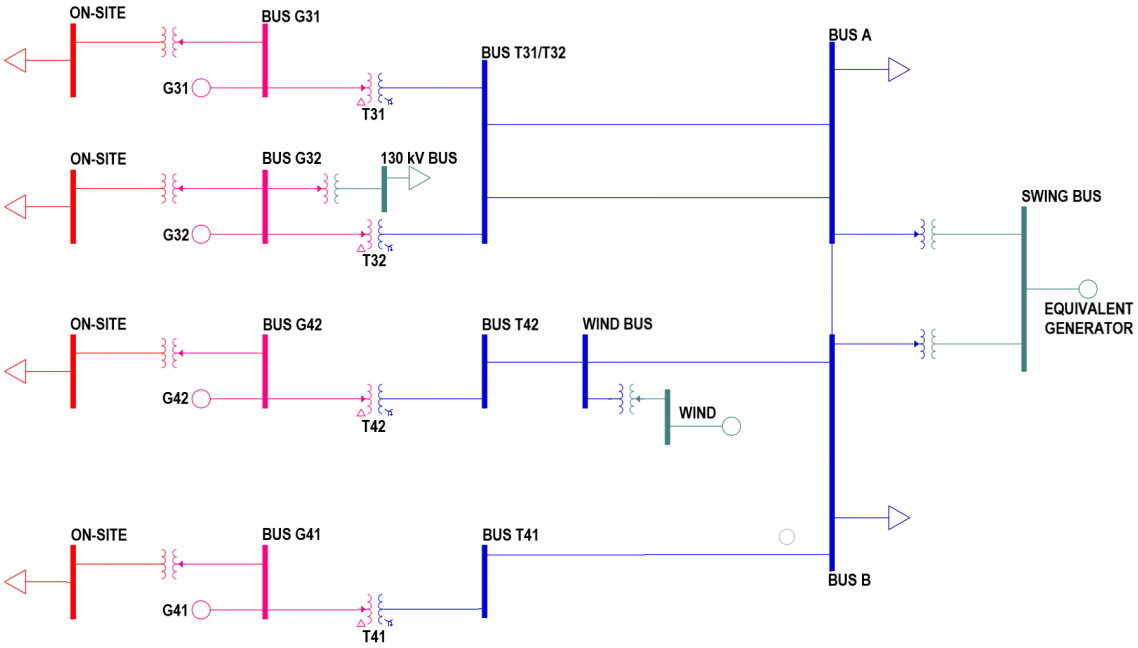

Figure 6.1: The single-line diagram of the "Standard" model used to simulate the interactions between Ringhals and the WPP during faults.

To the left in the model in Figure 6.1, there is a transformer going from rated generator voltage (21.5 kV) to 6 kV and feeding a large induction machine meant to approximate the local grid at the Ringhals compound. To the right of the Ringhals generators, there is one step-up transformer per generator and then the 400 kV transmission lines. At the other end of these lines, there are buses with connected loads and step-down transformers connected to a generator which is meant to approximate the extended grid. It is modeled with a very large power rating and an inertia constant (H) set to infinity, as frequency will not be covered in these simulations. The transformers from the equivalent generator will limit the short-circuit current.

At 20 % of the line connecting transformer T42 to bus B, a wind bus has been added which does not exist as of now. This bus is meant to be where the WPP is thought to connect to the 400 kV grid, according to [8]. The impedance introduced by a subsea cable is disregarded in this project, although as the impedance is very low compared to, e.g, a transformer, the difference in result should be very small. A connection like this, as seen in Figure 6.1, loads the line very highly, which results in high reactive power losses. Connecting the WPP to both lines heading towards bus B would better distribute the load and reduce the reactive power losses, this alternative model, named "Parallel", is shown in Figure 6.2. However, this is also a bad alternative since the reactance of the high voltage transformers T41 and T42 is lower than T31 and T32, so a connection where G41 and G42 can feed each other with fault current during an internal fault at either G41 or G42 could be dangerous and result in a situation where the fault current flowing in to Ringhals is too large and damages components. A third option will also be considered where the WPP

is connected to the line that is now used for G42 and G41 and G42 will share one of the transmission lines towards bus B, this alternative model, named "Own line", is shown in Figure 6.3. G41 and G42 sharing one transmission line was the configuration before the decommissioning of R1 and R2, which has the disadvantage that both generators could be disconnected from one single fault.

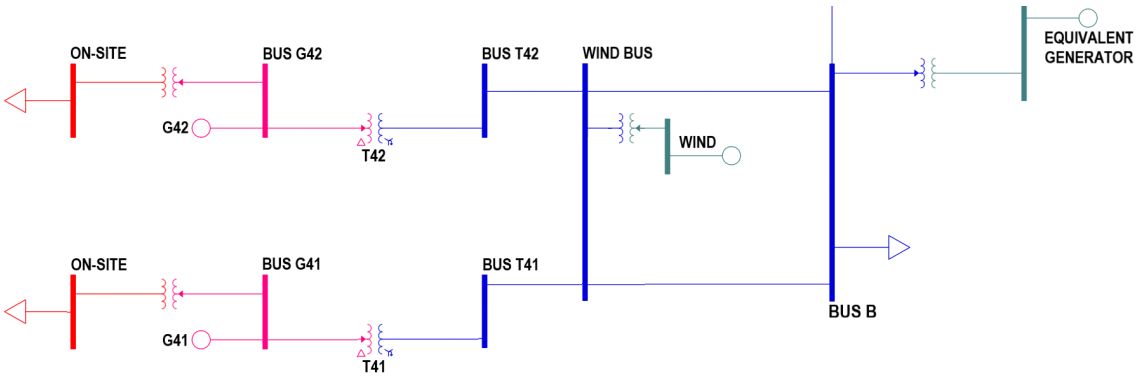

Figure 6.2: Alternative model "Parallel" (cropped).

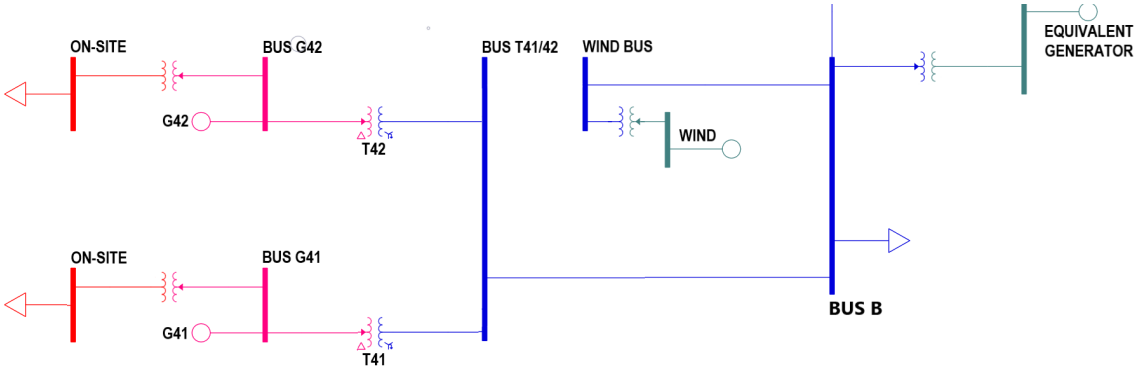

Figure 6.3: Alternative model "Own line" (cropped).

An error in the models used is that the 130 kV connection to G32 is in reality connected as a step-down transformer from the 400 kV side at bus T31/T32. Although this difference should not have impacted the result in a major way.

6.2 Verifying the Ringhals model

To verify that the PSS/E model of Ringhals power plant was correctly implemented, a comparison with approved Ringhals models was made to the "Standard" model without the WPP. Two different approaches were used. First, short circuit currents at a number of buses in the model were calculated and compared with the values in [37]. The second method was to compare CFCTs with the values from [38]. The maximum fault currents and the CFCT were similar to the approved models, as can be seen in Table 6.1 and 6.2, hence no particular changes were made.

Table 6.1: Maximum fault currents with saturated subtransient impedance.

Bus	Values from our model (kA)	Values in Ringhals report (kA)	Deviation (%)
G32	147.7	147	+0.47
G42	153.4	150	+2.27
B	28.12	28.3	-0.64
A	24.74	25.5	-2.98

To extract short circuit currents from PSS/E, the function "SCMU" was used and a bolted 3-phase to ground fault was applied at certain buses in the system and the different short circuit contributions were then added up and compared with the corresponding values in SvKs model of Ringhals and the surrounding grid. The SvK model used for comparison had a more extensive grid so in some cases, the contribution from two or more buses was added together and compared with the contribution from the equivalent generator in the model used in this project.

The next verification step was the CFCT. To evaluate this, several 3-phase to ground faults with different duration were placed at bus B. When the fault resulted in a situation where one or several of the angles of the Ringhals generators went to infinity the duration of the fault was lowered until a fault duration in which none of the machines lost synchronism was found. This was seen to be the system CFCT. The value acquired was then compared with the CFCT given by an internal Ringhals report where a model from SvK was used [38]. The grid configuration of the SvK model was the same as the "Standard" model without the WPP, but more extensive. All transmission lines were in use and the generators at Ringhals were evaluated for three different states of active and reactive power productions. The model used in this report had similar generator operating conditions, all four Ringhals generators had a maximum active power production and a reactive power production ranging between 153 and 171 MVar for the different generators. As can be seen in Table 6.2, the value for the model of Ringhals used in this project corresponds well to the values of the SvK model. SvK gives a range since their model was evaluated for three different load flows, whereas the model used in this project was only evaluated for one operating condition.

Table 6.2: Comparison of CFCT for G41 and G42 for SvK model and the "Standard" model without the WPP.

Model	CFCT for bolted fault at bus B (ms)
SvK	250-276
Standard model without wind	258

What can be seen in Table 6.2 is that the CFCT for a bolted 3-phase fault at bus B given by the "Standard" model is in the reported range of the SvK model. The model is deemed to be of acceptable quality, although, none of the results acquired

from the model can be seen as a fact, but they will at least give some idea of what can be expected if a WPP is connected close to Ringhals.

6.3 Modelling of wind power plant

To model a WPP, a renewable generator model and a step-up transformer are used in PSS/E. The reactance of the transformer is set to 0.15 p.u since this is a generic value used for step-up transformers in well-known models such as the Nordic32 model. The size of the generator is set according to the approximated installed power 1500 MW where this value is set as the maximum active power and the maximum reactive power is set to one third of the maximum active power, 500 MVar. Since the WPP considered in this project is of Type 4 the ability to provide reactive power is good, however, as stated before, there are not any specific demands in the grid code regarding reactive power injection from a WPP during faults so it cannot be assumed that the WPP will provide any reactive power during certain events.

A Type 4 WPP will behave differently during a fault compared to a SG. A SG can output a large current of about ≈6 p.u during a short bolted fault which helps with maintaining the voltage and the stability of the grid. A converter will be limited in this regard and is only likely to output 1-1.2 p.u of rated current during a fault where the grid voltage drops [39].

To model a wind generator in PSS/E, several models are implemented for dynamic simulations in PSS/E. One model simulates the converter used for the WPP, another simulates the electrical control, one simulates the auxiliary control and a third simulates a simple drive train model of a Type 4 WT. A thorough review of these models is outside the scope of this project, but a simplified figure that shows how the different parts are connected is shown in Figure 6.4. Some parts of the electrical control model need to be explained to understand the results so this will follow below.

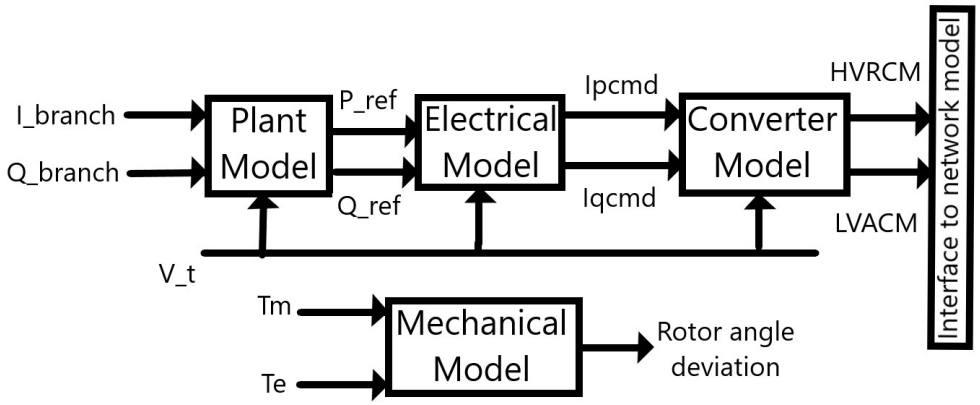

Figure 6.4: A simplified overview of the Western Electricity Coordinating Council (WECC) wind models applied in this project.

I_{branch}, Q_{branch}, V_t, T_m and T_e come directly from PSS/E. Many of the models have more inputs, for example different reference values, these have been excluded from the figure to make it less cluttered. The acronyms HVRCM and LVACM stands for "High Voltage Reactive Current Management" and "Low Voltage Active Current Management" respectively. The mechanical model was seen unnecessary and indeed the rotor angle deviation was never used for plotting or as an input to any other model. The reason it was included was that the program would not function without it.

6.3.1 The electrical model

The electrical model, visualized in Figure 6.5, regulates the output of active and reactive current. When the voltage at the WPP bus dips to a value equal to or lower than 0.9 p.u "Iqinj" will go from zero to "Iqv" which boosts the reactive current out from the model. Since it is not known how strong a potential fault current injection controller will be in the case of the WPP connected close to Ringhals two different strengths of the controller have been evaluated. Changing the value of gains Kqv, Kvp, and Kvi was identified as an effective way of achieving a stronger and weaker fault current injection during a fault.

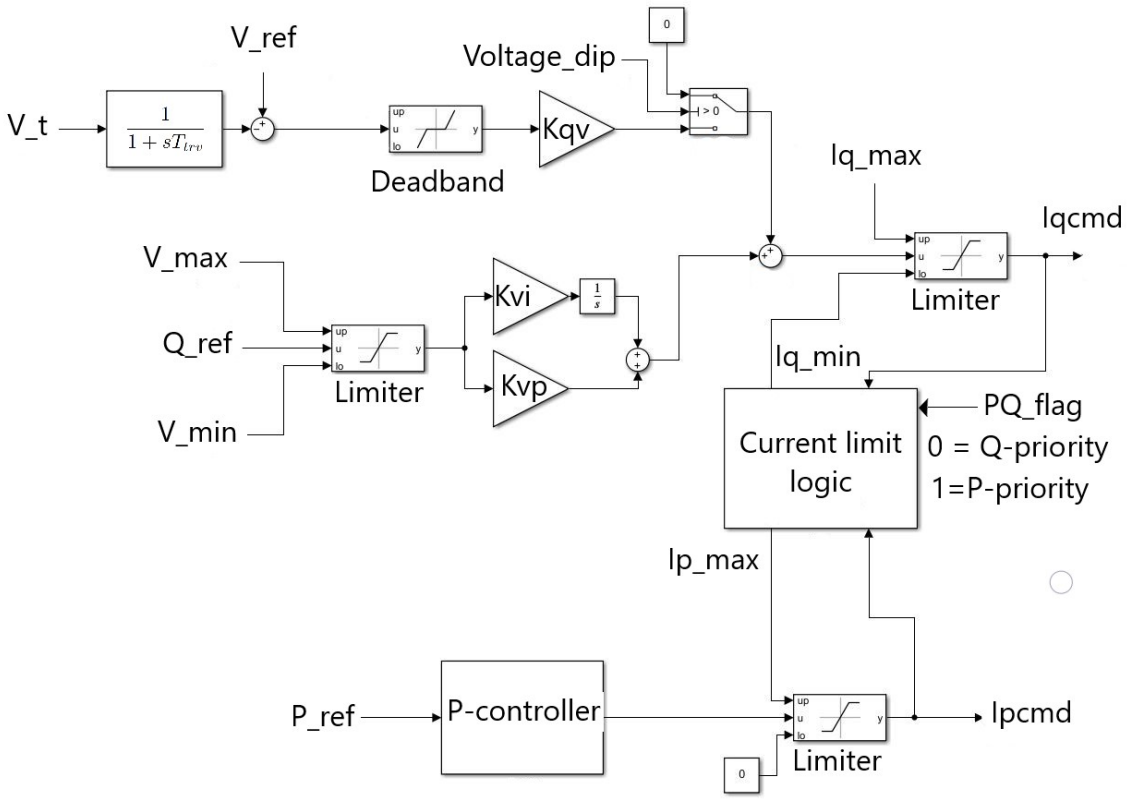

Figure 6.5: A simplified version of the electrical model used in the project. The actual model has a larger number of inputs and its functionality is dependent on the setting of a number of "flags" that have been left unchanged.

When a voltage dip has occurred the value Iqinj is added to the output from the middle part of the controller which regulates the reactive power during steady-state operation. This new value is called Iqcmd and is sent to the converter model. The values are also needed for the current limit logic block.

The block called "current limit logic" in Figure 6.5 works in the following way: The maximum current output, I_{max}, has been defined in the dynamical model, in this case, it is set to the expected maximum value 1.2 p.u. How this value is used for calculating limits for active and reactive current depends on if the controller is set to prioritize reactive current (Q-priority) or active current (P-priority).

- Q-priority: The upper and lower limits for active and reactive current are set in the following way and order

$$I_{qmax} = I_{max} \tag{6.1}$$

$$I_{qmin} = -I_{max} \tag{6.2}$$

$$I_{pmax} = \sqrt{I_{max}^2 - I_{qcmd}^2} \tag{6.3}$$

$$I_{pmin} = 0 \tag{6.4}$$

  where I_{qcmd} is the instantaneous reactive current output from the controller. I_{qmax} and I_{qmin} are the maximum and minimum reactive current limits, respectively. I_{pmax} is the active current maximum value.

- P-priority: In this case current limits are set using the following equations in the following order

$$I_{qmax} = \sqrt{I_{max}^2 - I_{pcmd}^2} \tag{6.5}$$

$$I_{qmin} = -1 \cdot I_{qmax} \tag{6.6}$$

$$I_{pmax} = I_{max} \tag{6.7}$$

$$I_{pmin} = 0 \tag{6.8}$$

  where I_{pcmd} is the instantaneous active current output from the controller. I_{pmin} is the minimum active current.

To simulate a strong and a weak fault current injection respectively a few constants in the electrical model of the WPP have been varied. Table 6.3 shows the changed constants and the assigned value in both cases.

Table 6.3: Changed gains in the electrical model for strong and weak fault current injection.

Parameter	Value for strong	Value for weak
Kqv	2	1
Kvp	2	0.1
Kvi	0.5	0.025

In Figure 6.6 and 6.7 the amplitude of the fault current injections for the two different controller strengths are shown. Only the reference currents are given as outputs from PSS/E so the actual currents have been calculated using the equations

$$I_{Active} = \frac{P_{WPP}}{\sqrt{3} \cdot V_{WPP}} \tag{6.9}$$

$$I_{Reactive} = \frac{Q_{WPP}}{\sqrt{3} \cdot V_{WPP}} \tag{6.10}$$

where V_{WPP}, P_{WPP}, and Q_{WPP} is the voltage at the WPP and the active and reactive power output from the WPP. The currents were then converted into their p.u values through

$$I_{ActiveP.U} = \frac{I_{Active}}{I_{base}} \tag{6.11}$$

$$I_{ReactiveP.U} = \frac{I_{Reactive}}{I_{base}} \tag{6.12}$$

I_{base} is the base current for the WPP base, which was calculated using the equation

$$I_{baseWPP} = \frac{1500MVA}{\sqrt{3} \cdot 400kV} \tag{6.13}$$

1500 MVA is the rated apparent power for the WPP and 400 kV is the rated voltage.

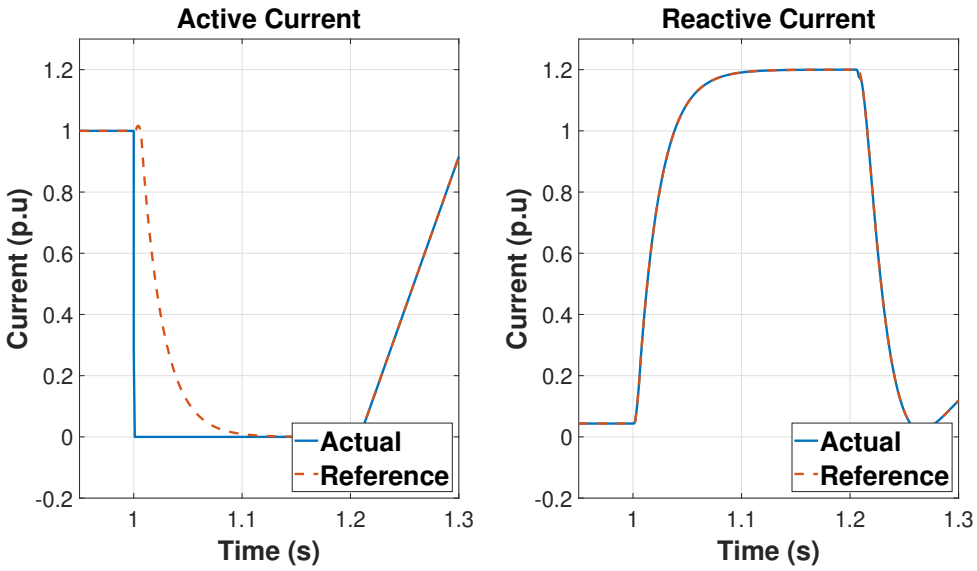

Figure 6.6: Active and reactive current injection from a strong controller during a 200 ms bolted fault at bus B.

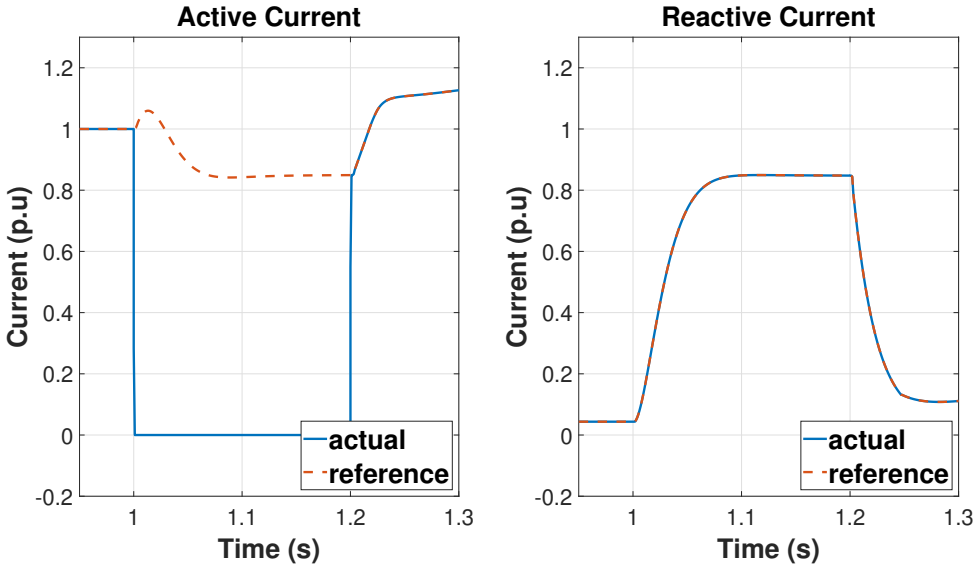

Figure 6.7: Active and reactive current injection from a weaker controller during a 200 ms bolted fault at bus B.

From Figure 6.6 and 6.7 it can be seen that in the case of strong injection, the controller quickly increases reactive current output until it reaches its limit of 1.2 p.u, which forces the active current down to zero. In the case with weaker injection, the controller only outputs approximately 0.8 p.u of reactive current, the active current reference remains high but the actual output has collapsed since the voltage is too low. How the voltage of generator G41 and G42 is impacted by this change in the "Standard" model is shown in Figure 6.8.

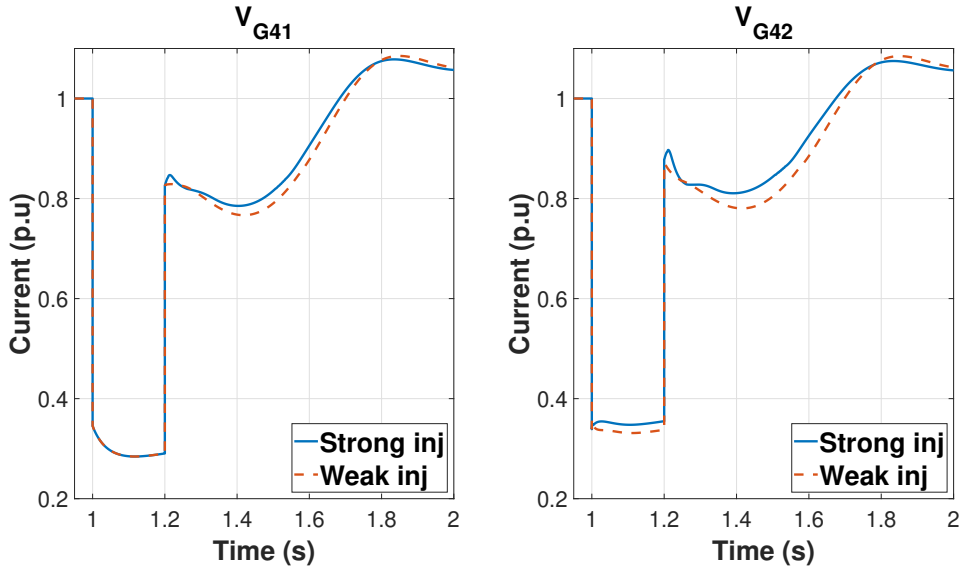

Figure 6.8: Voltage at G42 and G41 during a 200 ms bolted fault at bus B.

G42 and G41 were chosen for plotting since they are closer to the WPP than G31 and G32 meaning that they are most affected by it. We can see that the magnitude

of fault current injection from the WPP increases the voltage more of the closest generator, G42, compared to G41. But nothing too extensive happens in either case, a larger impact would be seen if the grid was weaker.

6.3.2 P-priority & Q-priority

As stated in the beginning of this chapter, a demand for fault current injection is yet to be made. When such a demand is made, a decision must be made whether active or reactive current should be prioritized. In the previous subsection focus was put on reactive current, here focus will be made on what the different effects are if an active current is called for instead. It is worth mentioning that reactive current injection is the most frequent practice [39].

To evaluate this the controller in the electrical model is kept at the setting previously described as "strong" but the controller will be set so that active current has priority over reactive current during the fault. A bolted fault at bus B is applied and the outputs from the WPP are compared in Figure 6.9 below. The model "Standard" was used though out this subsection.

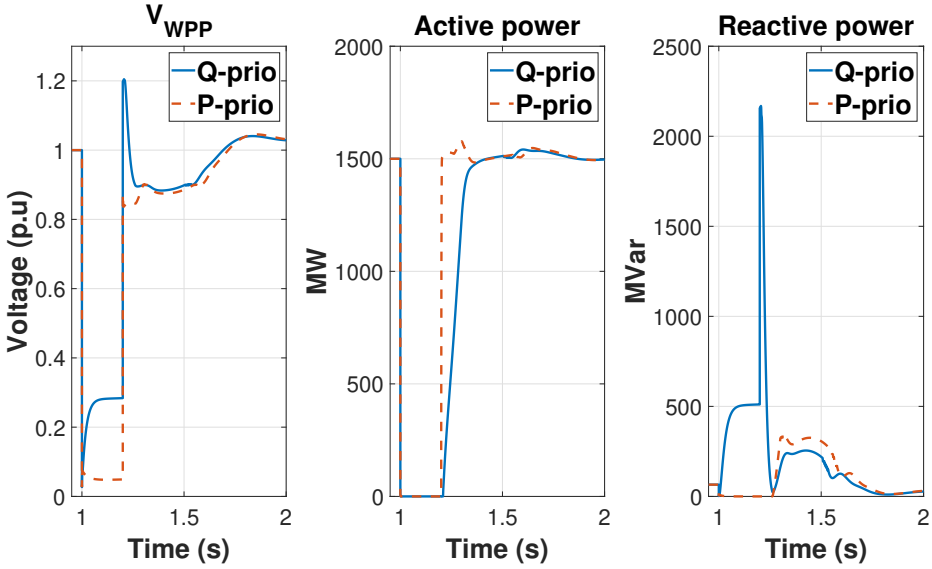

Figure 6.9: Voltage, active and reactive power injection at WPP PCC, during a fault for the controller using either P- or Q-priority.

If Q-priority is considered first, the controller prioritizes a reactive current which keeps the voltage considerably higher, this priority results in an active power output of zero. For the case with P-priority, the lack of reactive current response means that the voltage falls lower, so even though active power has priority there is very little active power. The active power output drops from 1500 MW to 70 MW during the fault. A production of 70 MW instead of 0 MW as is the case for the case with reactive priority will not help with maintaining the frequency in a major way, while the reactive current could have a major impact on the local voltage during a fault. Although, once the fault is cleared, the active power output will more quickly

reach nominal value in the case of P-priority which could be beneficial for the WPP and the system in terms of frequency. For the Q-priority there is a slight delay in the active power recovery since the reactive power will have priority as long as the voltage at the PCC is below 0.9 p.u. This means that after the initial transient after the fault is cleared the voltage drops slightly below 0.9 p.u and the controller will make sure that active power production is limited to prioritize reactive power, as opposed to the P-priority case where the WPP starts producing large amounts of active power as fast as possible. Figure 6.10 below shows the absolute value of the current output from the WPP during the fault for the two different controller settings.

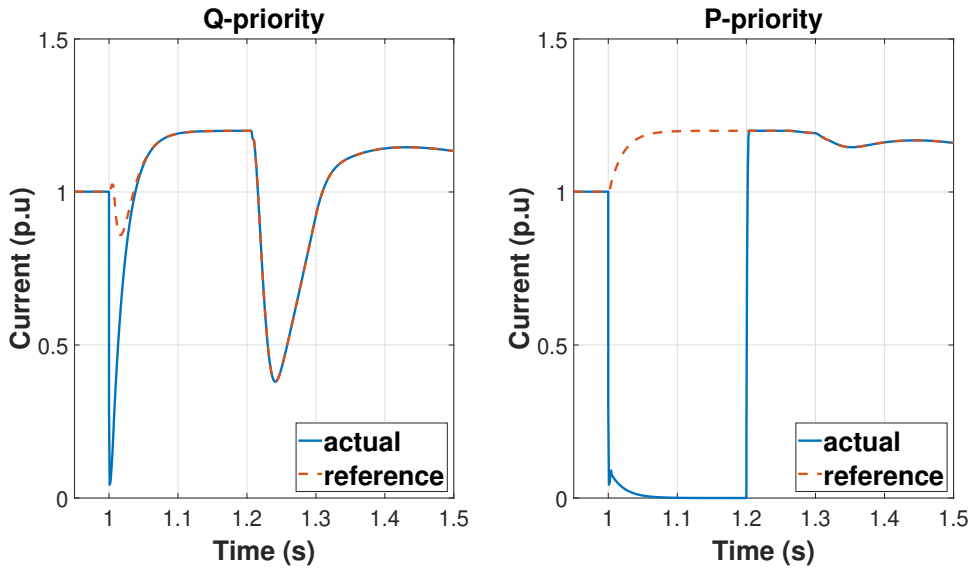

Figure 6.10: The absolute value of the current from the WPP during a fault for the controller using either P- or Q-priority

Transients found in Figure 6.10 for Q-priority at one second happens when the controller quickly tries to limit active current output from its maximum down to zero while also increasing reactive power from close to zero to the highest value possible with the given voltage at the bus. It can also be noted that once the fault is cleared at 1.2 seconds, the current drops to 0.2 p.u for Q-priority, it seems as this is because the WPP can change reactive current output faster than active current output, which can be seen in Figure 6.9.

For the active current priority case the current fails completely to follow the reference. This happens when the controller sets the maximum active current equal to 1.2 p.u and the reactive current to zero but the voltage is very low. For very low voltages the WPP fails to produce any active power. Using a controller that prioritizes active current is seemingly without benefit in this case since the result is neither active nor reactive power, but no power at all.

If the fault is applied slightly further away electrically, namely at the high voltage side of the transformers T31/T32 in Figure 6.1, the voltage at the PCC for the WPP

does not drop as low and the effects of prioritizing are slightly different as can be observed in Figure 6.11.

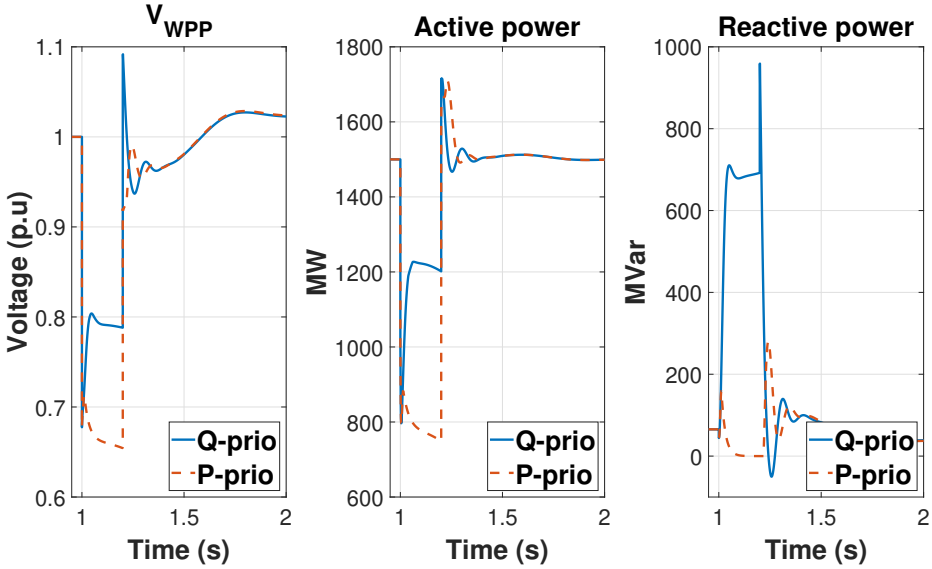

Figure 6.11: Voltage, active and reactive power injection at WPP PCC during a 5 Ω (reactance) fault at bus T31/T32 for either P- or Q-priority.

In the case of P-priority, due to the voltage being higher than in the previous case, the active power is approximately 0.3 p.u. at its lowest point. The reactive power is however forced down to zero. For the Q-priority case, the voltage is kept significantly higher due to the large amount of reactive power. This in turn lets the WPP transmit more active power which makes this priority a win-win over the P-priority case. The delay in active power ramp up is not seen for Q-priority in this case because the voltage does not drop below 0.9 p.u after the fault has been cleared. Whenever the voltage is above 0.9 p.u the reactive power priority is disabled. The conclusion that can be drawn from this simulation is that a demand that calls on active fault current injection instead of reactive is very unlikely, unless there are other factors at play that cannot be investigated in this model or with this method.

6.3.3 No fault current injection

To evaluate a situation where there is no fault current injection, I_{max} is set to 0 during the dynamic simulation and then set to 1.2 p.u again when the fault is cleared. This means that both active and reactive power will drop to zero and return to pre-fault values as fast as the controller can manage once the fault has been cleared. The resulting voltage at bus G42 is then compared with a case where the fault current injection is strong and reactive current is prioritized, as shown in Figure 6.12 for a bolted fault at bus B and in Figure 6.13 for a fault at bus B with a 5 Ω reactance added to simulate a fault further away from Ringhals and the WPP.

For both cases the "Standard" model was used but only the voltage from generator G42 is shown since, as seen in 6.8, the fault current injection is unable to impact

the voltage at G41 when there is a bolted fault between the WPP and G41. in the case plotted in Figure 6.13 the WPP impacted the voltage at G41 but only in a very minor way so it was not included.

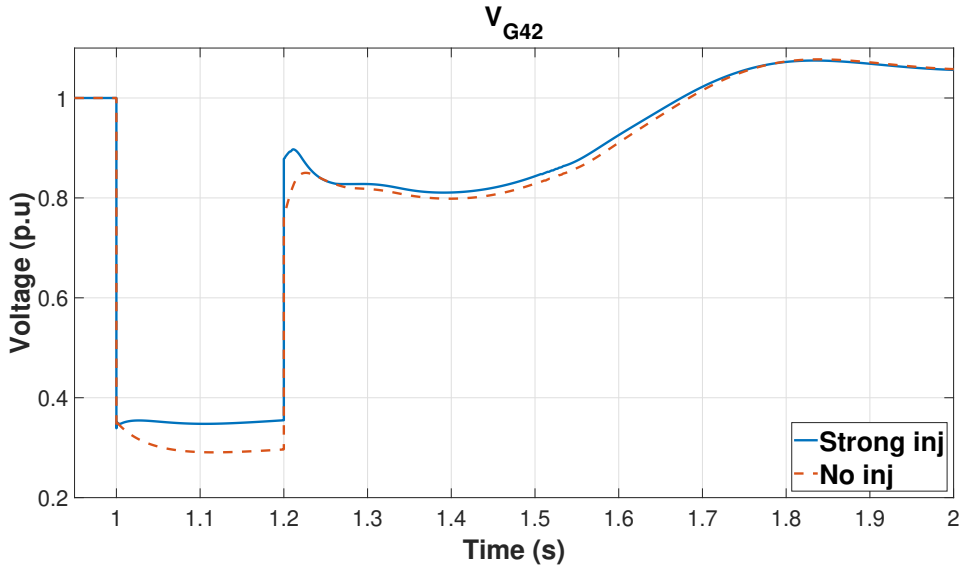

Figure 6.12: Voltage for G42 for a bolted fault at bus B, with and without fault current injection.

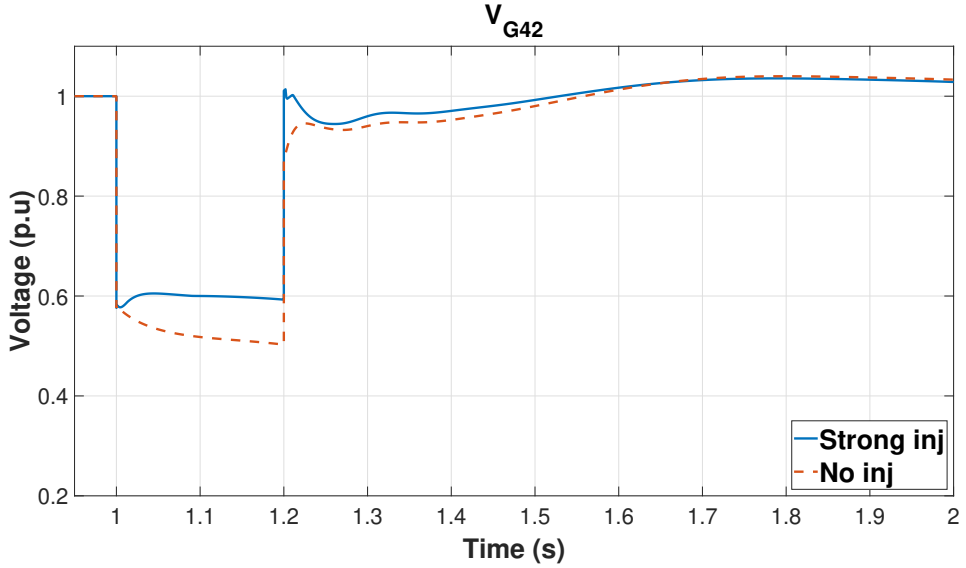

Figure 6.13: Voltages for G42 for a 5 Ω (reactance) fault at bus B, with and without fault current injection.

First of all, it can be noted no type of undervoltage protection in these or any later cases is considered in this report. In both fault cases the fault current injection from the WPP can help keep up the voltage at G42 due to the strong coupling. It is also obvious that the injection helps more in the case with added reactance because the retained voltage is higher so the same amount of reactive current gives a higher

reactive power. For the models "Parallel" and "Own line" the impact from the WPP will be distributed more evenly between G41 and G42 depending on the strength of the coupling between them and the WPP.

6.4 Tripping of wind power plant

In the case of a sudden disconnection of the WPP, a surplus or deficit of reactive power in the grid close to Ringhals could occur. At the same time, the loading of the transmission lines connected to bus B will also decrease, which means that they will consume less reactive power. Depending on how much reactive power the WPP is producing and how heavily loaded the lines are it is possible that the voltage could either increase or decrease in magnitude when the WPP trips. The worst-case scenario should be the one with the largest surplus or deficit of reactive power in the grid. When studying the effects on Ringhals of a disconnection of the WPP two different scenarios have been simulated which are presented below. Both active and reactive power have been varied.

- "Q deficit": The WPP is producing maximum amount of reactive power and a small amount of active power. To achieve this situation the scheduled voltage at the equivalent generator is set to 0.9 p.u. This creates a situation where the grid voltage is too low at many buses and both Ringhals and the WPP will start producing large amounts of reactive power to cope with this situation. Tripping the WPP in this situation would result in the largest possible deficit of reactive power, which could result in a voltage drop in the grid.

- "Q surplus": The WPP is producing maximum active power and consuming maximum amount of reactive power. To achieve this situation the scheduled voltage at the equivalent generator is set to 1.1 p.u. This creates a situation where the grid voltage is too high at many buses and consumption of reactive power is need. Tripping the WPP in this situation would result in the largest possible surplus of reactive power, which could result in a voltage increase in the grid.

PSS/E tries to find the most optimal solution for the reactive power output from the different generators in the model by taking many factors into account, such as transformer impedance. When the scheduled voltage at the equivalent generator is set to 0.9 p.u it results in a situation where all four Ringhals generators produces maximum reactive power (295 MVar), even at steady state, whereas the WPP only outputs around 250 MVAr (slightly higher or lower depending on which model is used). To override PSS/E the reactive power output from the WPP was locked to 490 MVar before the disconnection of the WPP, this emphasizes the impact of a WPP with a large capacity for reactive output.

A similar but opposite situation arises when the scheduled voltage at the equivalent generator is set to 1.1 p.u, the WPP only absorbs half of the reactive power that it could, so it has been set manually to -490 MVar (negative signifies consumption

instead of production). To clarify this further, Figure 6.14 shows the active and reactive power output from the WPP before and after tripping, for both cases.

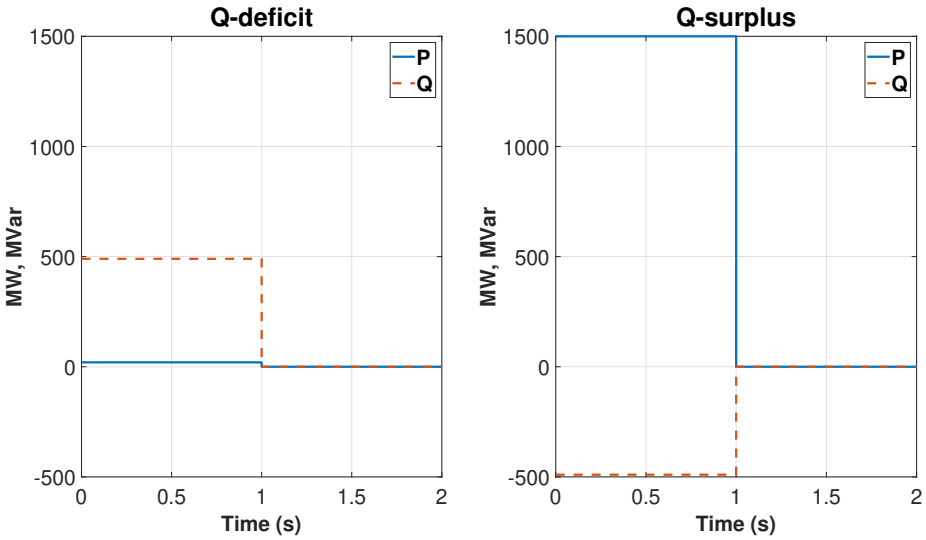

Figure 6.14: Active and reactive power output form the WPP for "Q deficit" to the left and "Q surplus" to the right.

It must also be stated that the load at bus B was removed in the case "Q deficit", where the WPP produced a negligible amount of active power, the load was set to 1500 MW for the case "Q surplus", when the WPP was at maximum active power output. This has been done for a number of simulations, and the reasons behind this choice are explained later in section 6.5. The two different scenarios have been applied to all three models, "Standard", "Parallel", and "Own line". Below in Figure 6.15 voltage at the Ringhals generators in the case of sudden disconnection of the WPP is shown for the case "Q deficit".

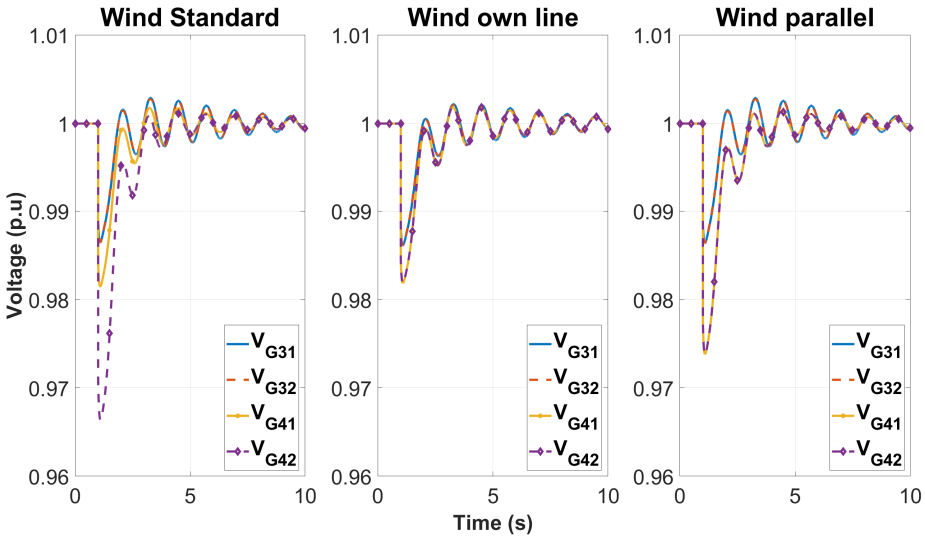

Figure 6.15: Voltage of generators at Ringhals when the WPP is disconnected in the case "Q deficit".

For the case with the "Standard" model the WPP is closely connected to G42, therefore, this generator is impacted the most and experiences the largest voltage drop. For the other two models the impedance between the WPP and generator G42 and G41 is identical, hence the voltage drop at the two generators are the same. Because of the grid configuration, generators G31 and G32 are affected in the same way in all three cases. To further investigate how Ringhals manages to handle this situation it is necessary to look at the reactive power output from the generators, which is shown in Figure 6.16.

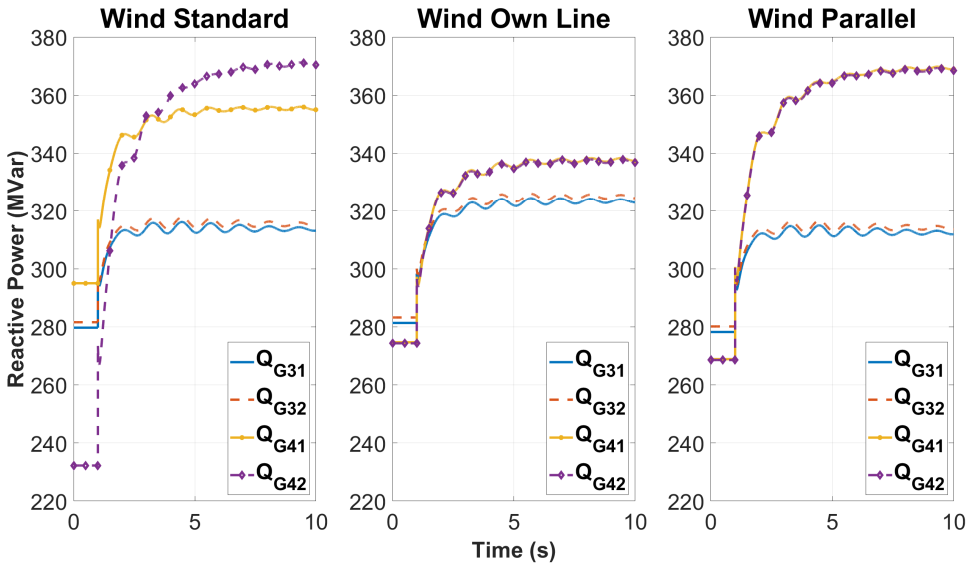

Figure 6.16: Reactive power production of the Ringhals generators when the WPP is disconnected in the case "Q deficit".

Figure 6.16 shows that all generators produce reactive power above the limit of 295 MVar once the WPP trips. In reality, the over exciter limiter of the generators would hinder this, although, the limiter is fairly slow and would only start to reduce the reactive power after a few seconds. When the limiter acts it does so by limiting the field current which limits the generators back EMF. This lowers the generators reactive output which would cause the voltage at the generators terminals to fall lower than what is shown in the graph. This voltage level can be found from a steady state solution in PSS/E, and was found to be 0.973 kV at G42, and 0.986 p.u at G32 for the model "Standard". It is also worth noting that since the limiter takes several seconds to act there are other shunt compensators connected in the nearby transmission grid to consider, which would impact the voltage. For the case "Q surplus", the resulting voltages at Ringhals generators is displayed in Figure 6.17.

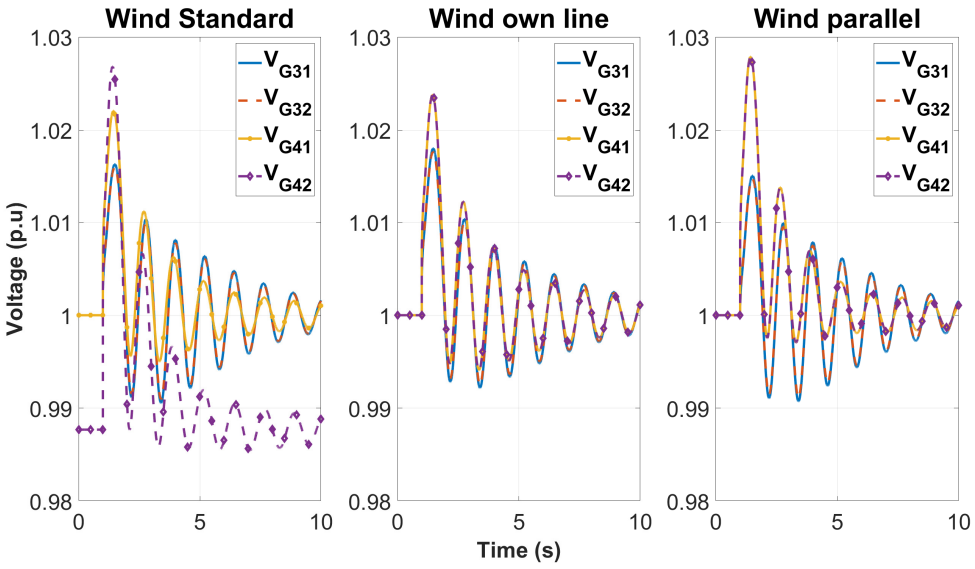

Figure 6.17: Voltage of generators at Ringhals when the WPP is disconnected in the case "Q surplus".

Figure 6.17 shows that G42 cannot manage to stay at 1 p.u at steady state. This would probably not be the case in reality since there is still unused reactive capacity in G42 in the simulation. The full reactive capacity would probably be used to keep the terminal voltage at G42 at 1 p.u, it is not entirely clear why the steady state voltage is lowered slightly in the simulation, perhaps it is to minimize losses in a very constrained grid. The magnitude of the voltage oscillations indicates that Ringhals and the surrounding grid can manage the disconnection without any major voltage deviations. The reactive power output for this case can be found on Figure 6.18.

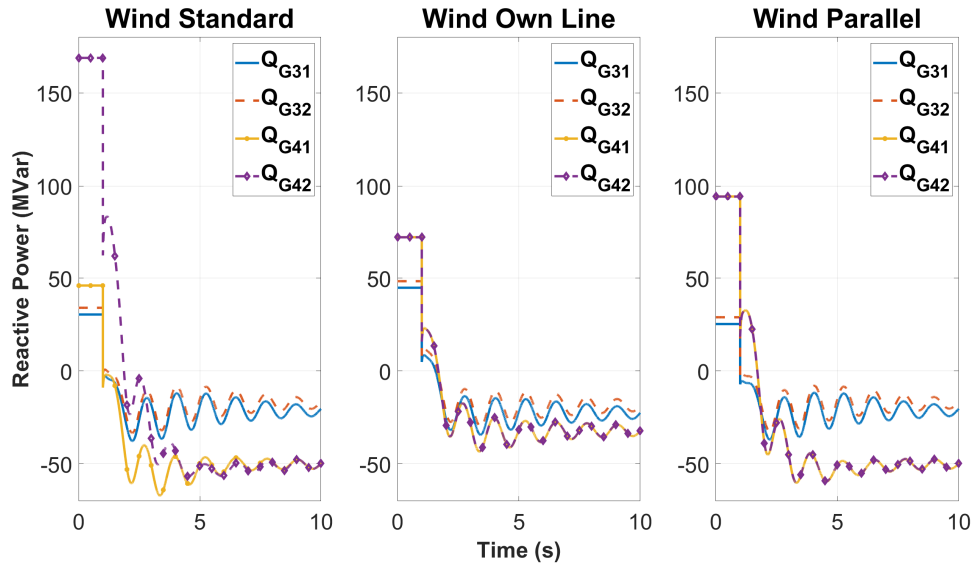

Figure 6.18: Reactive power production/consumption of the Ringhals generators when the WPP is disconnected in the case "Q surplus".

Figure 6.18 shows that the reactive power output from Ringhals is low before the

disconnection of the WPP for all cases and generators except G42 in the "Standard" case. What has happened in this case is that the large absorption from the WPP forces G42 to produce reactive power so that the voltage does not decrease too much. In the other cases the reactive power demand from the WPP is dispersed more equally among all other generators.

The fact that G41 and G42 is producing the same amount of reactive power for the two other cases is expected. The small difference in reactive power output from G31 and G32 exists because of the 130 kV grid which is connected to G32. As mentioned before, the 130 kV grid is just modeled as a constant 100 MW load behind a step-up transformer which is not actually the case in reality. It is the reactive power consumption due to losses in this transformer that forces G32 to produce slightly more reactive power than G31.

6.4.1 Fewer generators connected to the grid

During refueling or large repairs of a nuclear power plant the reactor must be shut down so that maintenance can be done. In this section, the previous two cases are evaluated again but with G31 and G32 disconnected in one case and G41 and G42 in the other case. This will make the local grid more vulnerable to voltage fluctuations.

The first scenario is when R3 is down for maintenance so G31 and G32 are disconnected from the grid. Since the resulting voltages at the buses for G31 and G32 versus the voltages at G41 and G42 are quite different they have been plotted in two different figures. Figure 6.19 shows voltages at the G31 and G32 buses, whereas Figure 6.20 shows the voltages for G41 and G42 both for the case "Q deficit".

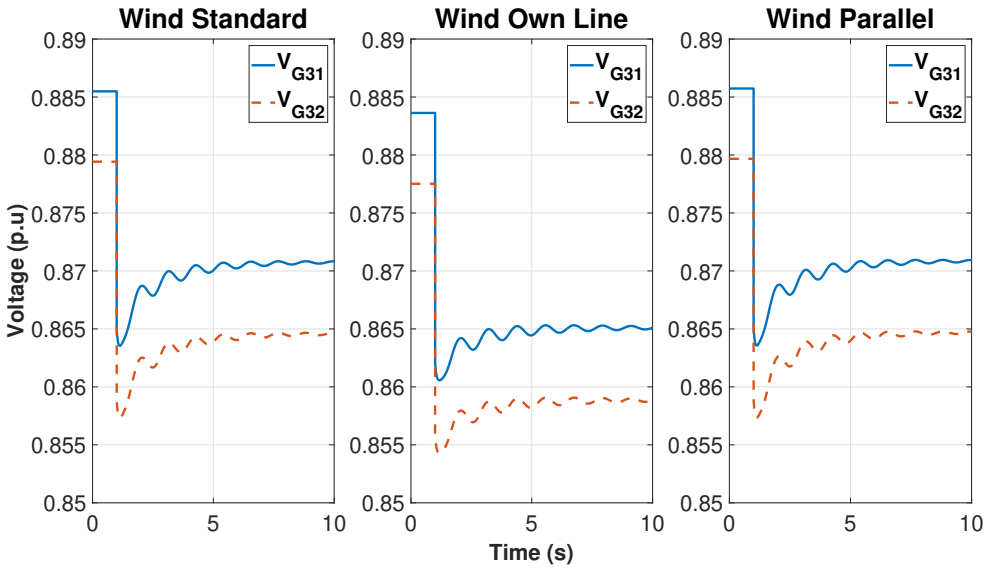

Figure 6.19: Voltage of G31 and G32 when the WPP is disconnected in the case "Q deficit". G31 and G32 are disconnected.

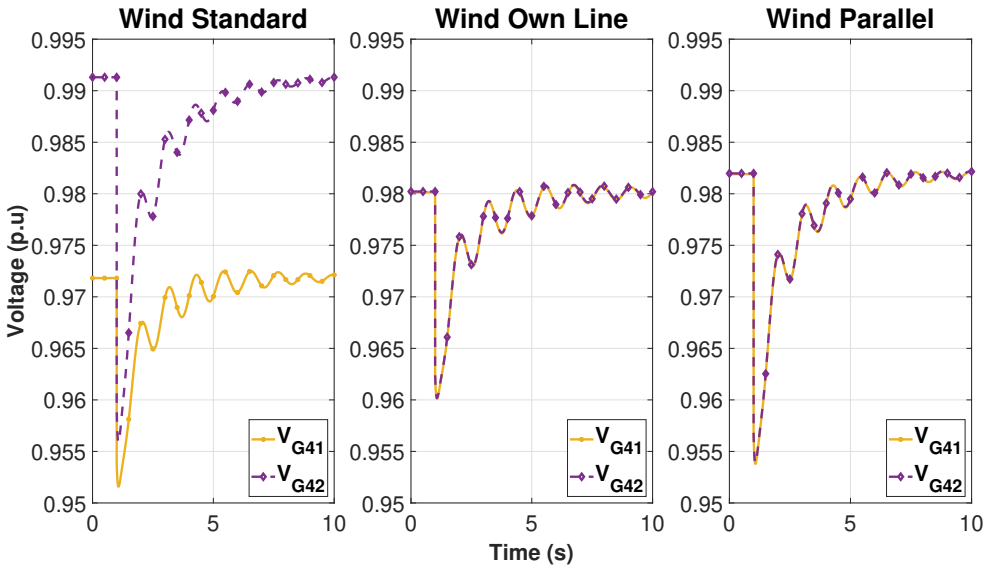

Figure 6.20: Voltage of G41 and G42 when the WPP is disconnected in the case "Q deficit". G31 and G32 are disconnected.

When studying Figure 6.19 it is crucial to remember that 0.0885 p.u is a quite unrealistic grid voltage that is only used as a worst case that most likely has its origin in the very basic model of the 130 kV grid. Even though the voltage at the equivalent generator is set to 0.9 p.u, the large reactive power output from G41, G42 and from the WPP almost manages to keep the voltage at 1 p.u for all cases before the disconnection. Naturally, there is a slight difference between the voltages for the model "Standard", owing to the difference in electrical distance between the WPP and G41 and the WPP and G42. The reactive power output from these two generators must also be studied and is shown in Figure 6.21.

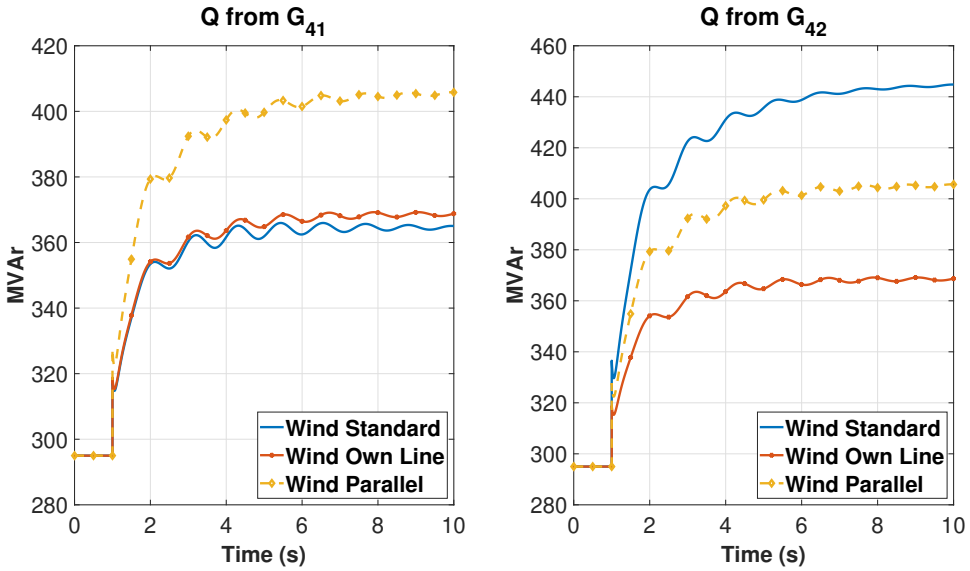

Figure 6.21: Reactive power production of G41 and G42 when the WPP is disconnected in the case "Q deficit". G31 and G32 are disconnected.

It is clear from Figure 6.21 that Ringhals would not manage to keep the voltage up for a longer period in this case. The reactive power output from the generators is at its maximum before the disconnection of the WPP and naturally must rise even higher after it has tripped. This would again cause the over-excitation limiter to act after a few seconds and the voltage would then decrease again. In the same was as before, this has been simulated to result in a steady state voltage of 0.943 p.u at G42, and 0.854 p.u at G32 for the model "Standard". While the voltage drop is small, it might still be necessary to create an agreement that limits the amount of reactive power supplied to the grid by the WPP, so that Ringhals can replace that supply if the WPP must disconnect from the grid.

For the scenario when G41 and G42 are disconnected from the grid, only the case "Q deficit" resulted in a simulation that converged. For the case "Q surplus" the simulation would not converge, and if the output is studied there are large oscillations in voltages even during steady state. This will not be the case in reality but perhaps the fact that the simulation did not converge can give an idea of how strained the grid would be in a case where the voltage in the grid has risen, G41 and G42 are disconnected and the WPP disconnects.

For the case that converged, "Q deficit", the resulting voltages at the buses for G41 and G42 are shown in Figure 6.22. Figure 6.23 shows the reactive power output from G31 and G32. The voltage for G31 and G32 were almost identical for all three models and looked very similar to Figure 6.20 so they are not plotted.

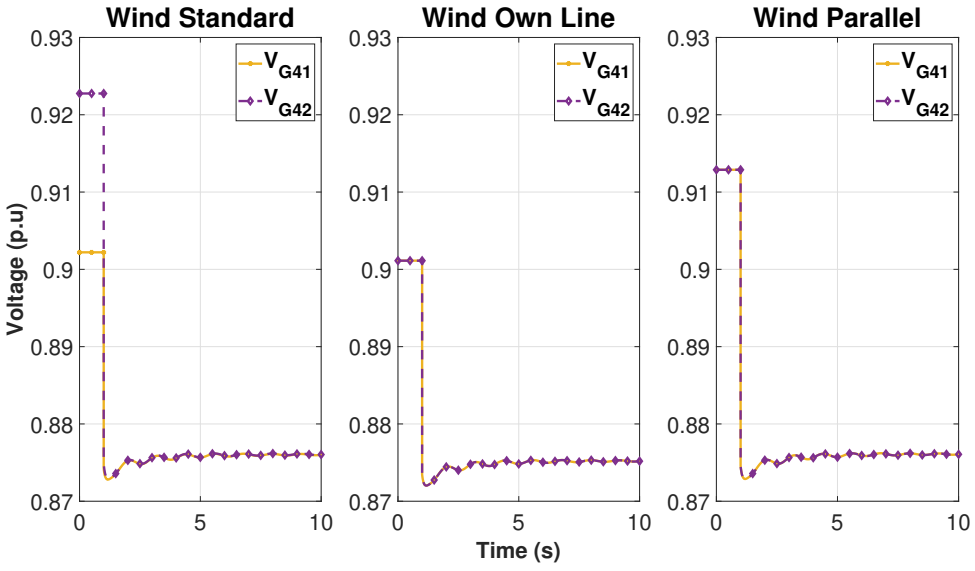

Figure 6.22: Voltage of G41 and G42 when the WPP is disconnected in the case "Q deficit". G41 and G42 are disconnected.

From Figure 6.22 it can be seen that even before the disconnection of WPP the voltage is at very low level, barely above the set voltage of the equivalent generator of 0.9 p.u. For the "Own Line" model the voltages are near 0.9 p.u, since there is a large electrical distance between any generator that could help keep the voltage up.

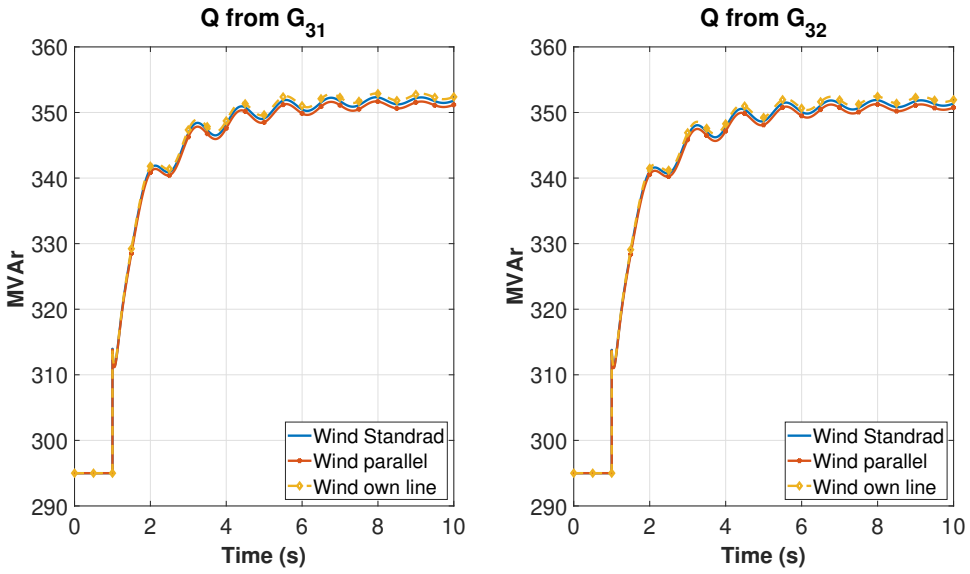

Figure 6.23: Reactive power production of G31 and G32 when the WPP is disconnected in the case "Q deficit". G41 and G42 are disconnected.

In Figure 6.23 just like earlier cases, the two generators operate at maximum reactive power output before fault and exceeds the limitations after the WPP has tripped. Once again, the over-excitation limiter would act, and the simulated steady state voltage was 0.871 p.u at G42 and 0.960 p.u at G32 for the model "Standard". This further exemplifies the need for reactive power coordination between the WPP and the grid.

6.4.2 Tripping after external fault

Another situation that can be of interest is when a fault at an external bus causes the WPP to disconnect from the grid, i.e., if the WPP cannot ride through the fault. In Figure 6.24 and 6.25, a case is shown for a 200 ms bolted fault at bus B, the WPP is disconnected at the same time as the fault is cleared. The three different models are shown together with the "Standard" model without the WPP.

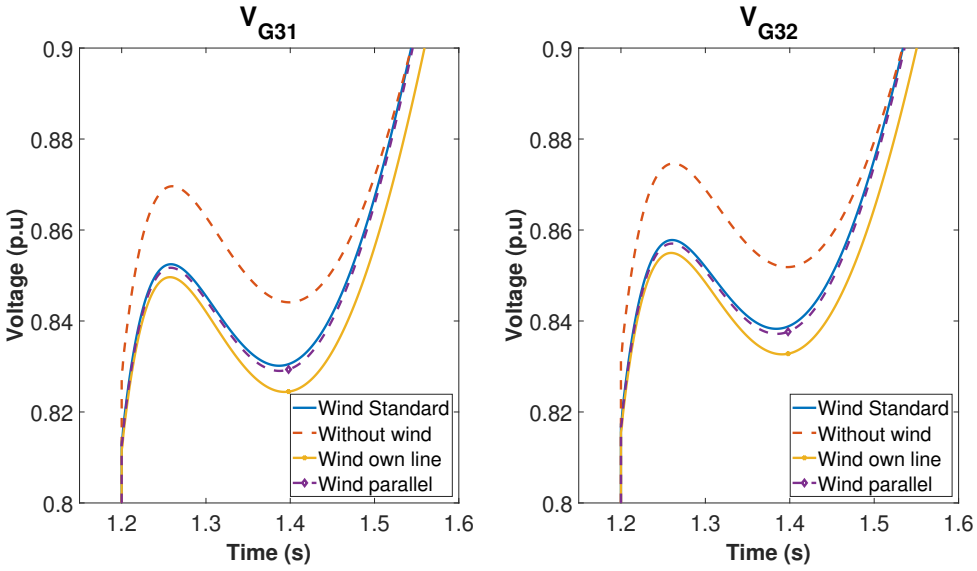

Figure 6.24: Voltages at G31 and G32 after a 200 ms bolted fault occurs at 1 second at bus B and the WPP disconnects from the grid at the same time as the fault is cleared.

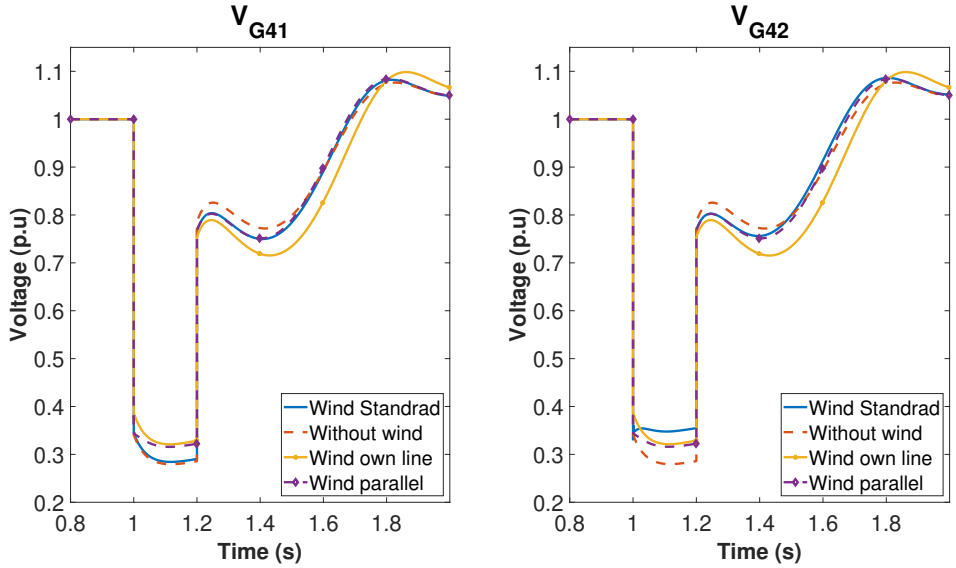

Figure 6.25: Voltages at G41 and G42 after a 200 ms bolted fault occurs at 1 second at bus B and the WPP disconnects from the grid at the same time as the fault is cleared.

In Figure 6.24 the result has been zoomed in to see the difference between the models. The graph only shows a small window of time just after the fault is cleared, since no difference in voltage between the different models occurred during the actual fault. The voltage returns quickest for the case where there is no WPP. This is most likely since with the WPP in the grid there is added impedance from, for example, the step-up transformer of the WPP which consumes reactive power. The

model without the WPP simply needs less reactive power to keep up the voltage.

The difference in voltage between the models is also small for G41 and G42 as seen in Figure 6.25, but there is a difference both during and after the fault due to the fault current injection from the WPP. In the "Standard" model, the voltage at G42 is kept high due to the strong coupling between that generator and the WPP. In the two other models with wind the coupling between the WPP and the two generators are equal, so the WPP helps with the voltages to the same degree. A slightly different case will appear if the disconnection of the WPP is placed earlier than the clearing of the fault. In Figure 6.26 the resulting voltages at G41 and G42 are shown when the WPP disconnects from the grid 50 ms after the occurrence of a 200 ms bolted fault at bus B.

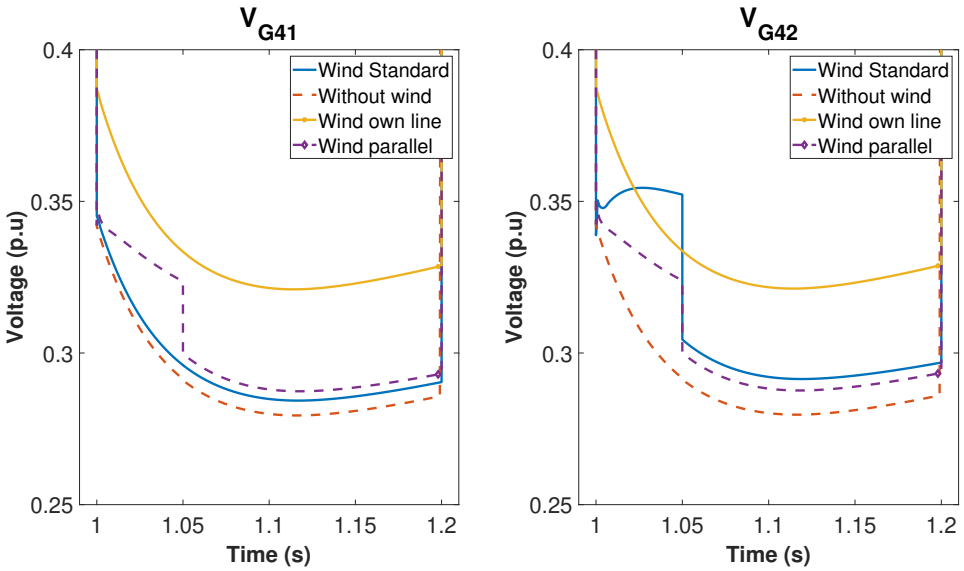

Figure 6.26: Voltages at G41 and G42 when a 200 ms bolted fault occurs at bus B and the WPP disconnects from the grid 50 ms after the occurrence of the fault

The graph in Figure 6.26 is zoomed in so that the difference in voltage during the fault can be studied easier. For G42 there is an obvious voltage drop when the WPP is disconnected. A similar appearance is also found for the model "Parallel". Interesting to note here is that due to the configuration of the grid in the model "Own line" it is impossible for the WPP to help keep the voltage higher regardless of its fault current injection abilities. There is no way for the WPP to send current to either of the generators since the voltage at bus B is zero. Even though the WPP is unable to help in this case the voltage is still higher for this model than for the model without the WPP, as both G41 and G42 are contributing with fault current through one transmission line.

6.5 Internal fault at Ringhals

If a WPP is connected to the surrounding grid the changes in behavior for Ringhals will not only be dependent on how the WPP interacts with the grid but also on how the WPP is connected to the grid and how the local grid is reconfigured due to the new installation. In Figure 6.27, a bolted fault is applied at G42 for all models, including the "Standard" model without the WPP, the resulting voltage at G41 is shown.

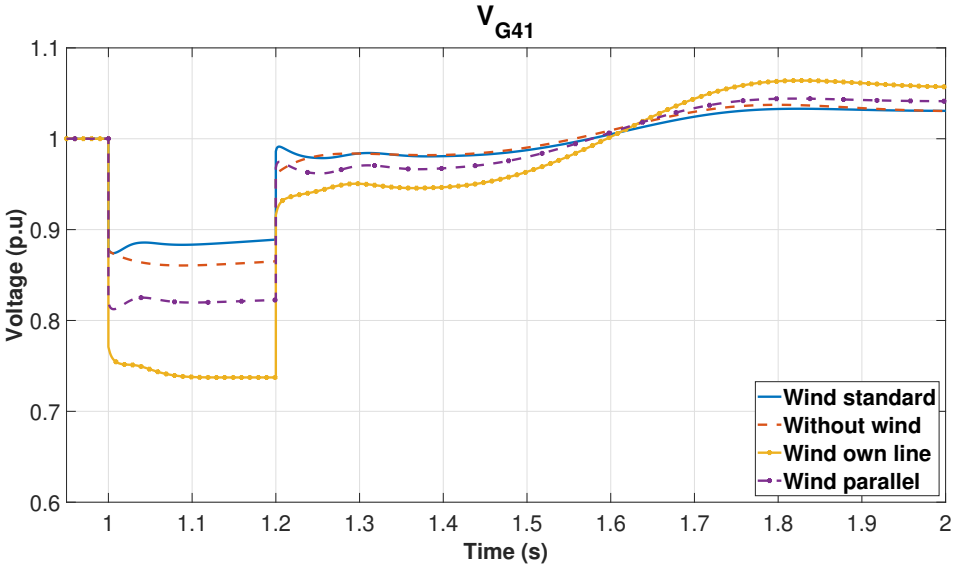

Figure 6.27: Voltage at G41 during a bolted fault at G42 for 200 ms. The active power generated by G41 is the same for all cases.

The graph shows that the voltage drops the lowest for the model "Own line". This is because the generators are now very closely coupled since the only impedance between the two are their transformers. A similar behavior occurs when the model "Parallel" is used, the impedance between G41 and G42 is in this case only the two transformers and 20 % of the transmission lines towards bus B. The significantly lower impedance for these two cases explains why the case without any wind has a higher voltage. The models "Standard" and "Without wind" shows some difference in voltage amplitude, this is due to the fault current injection from the WPP. Further, the rotor angle of G41 can be plotted for the different models, which is shown in Figure 6.28.

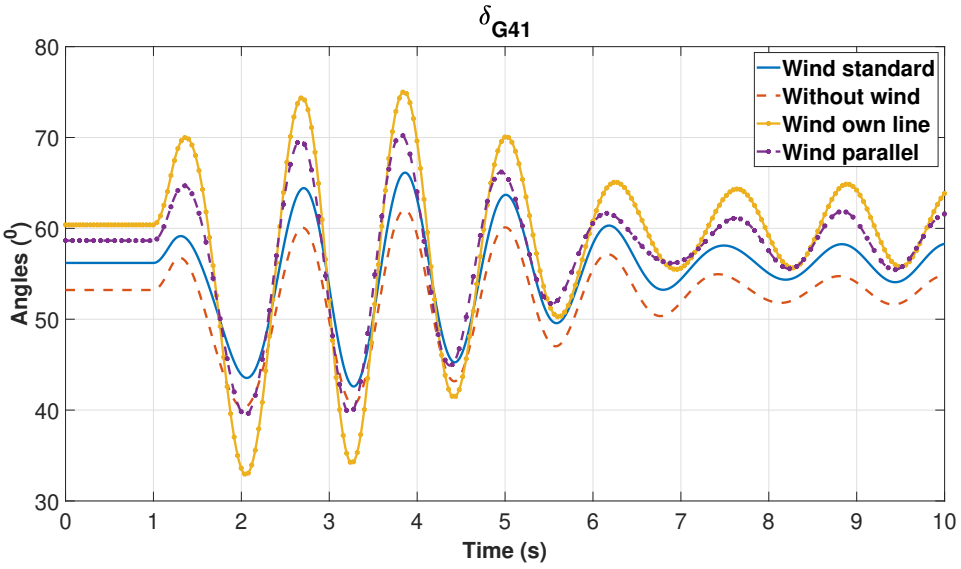

Figure 6.28: Rotor angles for G41s when there is a bolted fault at G42 for 200 ms. The active power generated by G41 is the same for all cases.

In this case we can see that the steady state rotor angle is lowest for the case without any wind power. This behavior can be explained by also looking at the steady state angle at the bus that Ringhals is feeding, bus B, which is shown in Figure 6.29

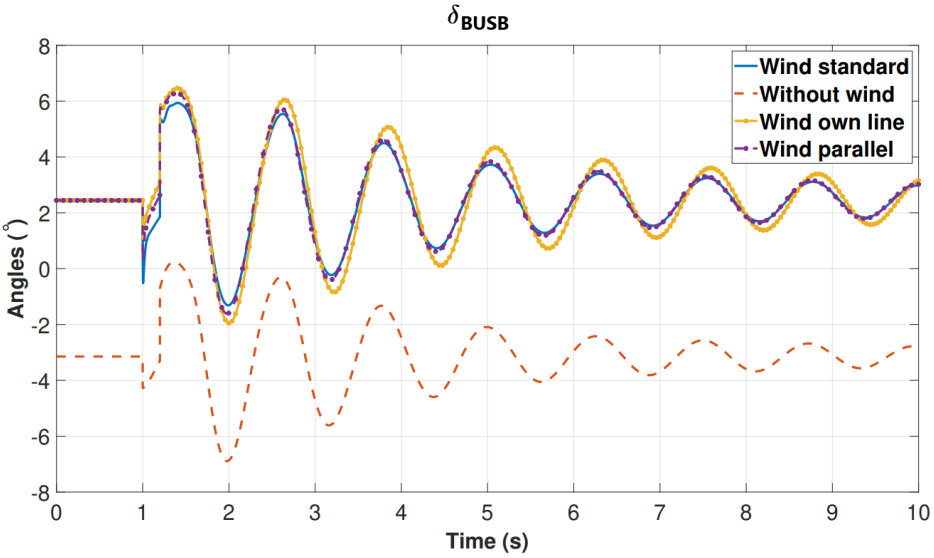

Figure 6.29: Bus angles for bus B when there is a bolted fault at G42 for 200 ms.

As can be seen in Figure 6.29 there is no noticeable difference between the cases where the WPP is connected, except that the oscillations are of slightly different size. The reason for the significant difference between the case without the WPP and the others is the loads in the model. In the model used there are three loads, one 100 MW at the 130 kV bus and two 1500 MW loads, one at bus A and one at bus B. For the models where the WPP is connected it is set to produce 1500 MW and Ringhals is producing 564 MW per generator, meaning that the entire production

of active power in the model is 3756 MW and the total consumption is 3100 MW. In this case equivalent generator which is set to represent the surrounding grid acts as a large motor and consumes the excess active power.

In the case where the WPP is not connected there is no generation surplus but a generation deficit in the system. Generations has shrunk to 2256 MW but the load is still 3100 MW so there is a deficit of 844 MW. The equivalent generator will then function as a generator and supply the missing active power. The angle at the equivalent generator bus (Swing bus) is always zero since it is the reference that all other angles in the system are compared to. Since power flows from a higher angle to a lower angle in a power system, the angle at bus B will either be positive if it is sending power to the equivalent generator or negative if it is receiving active power from it.

One way of correcting for this is to completely remove the load at bus B in the model without wind, so that a surplus of 656 MW is achieved in the model. The resulting angles at bus B and G41 in this case are shown in Figure 6.30 and 6.31 respectively.

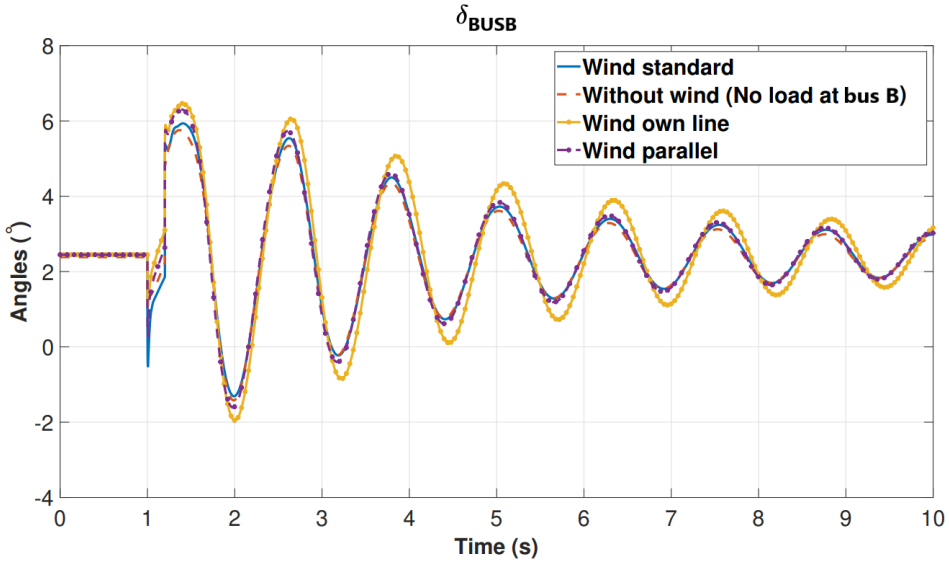

Figure 6.30: Angles for bus B after load correction during a bolted fault at G42 for 200 ms.

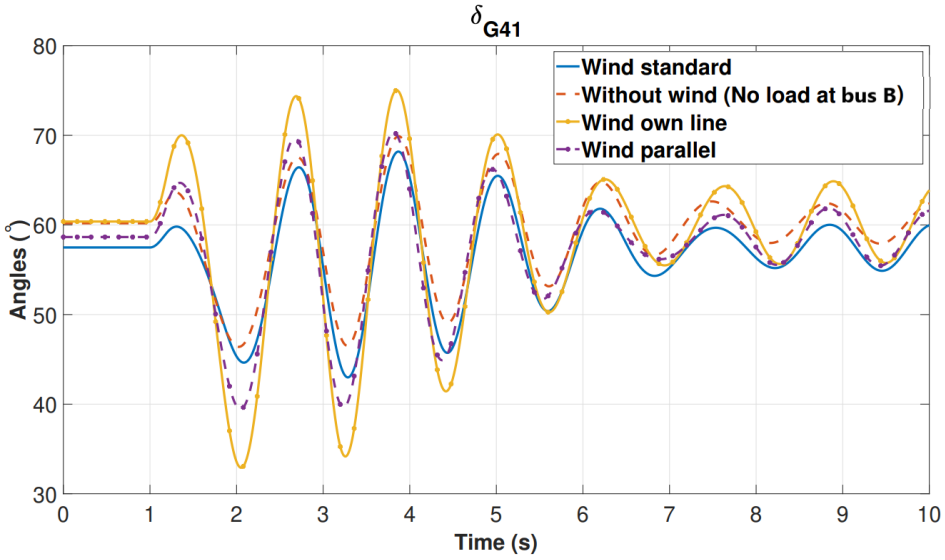

Figure 6.31: Angles for G41 after load correction during a bolted fault at G42 for 200 ms.

After the power flow in the model has been corrected the angles are now similar at bus B. To easily compare the size of the oscillation of the rotor angle for the different cases, the steady-state difference in rotor angle between the different models can be removed, which has been done in Figure 6.32 so that the size of the oscillations can be easily compared.

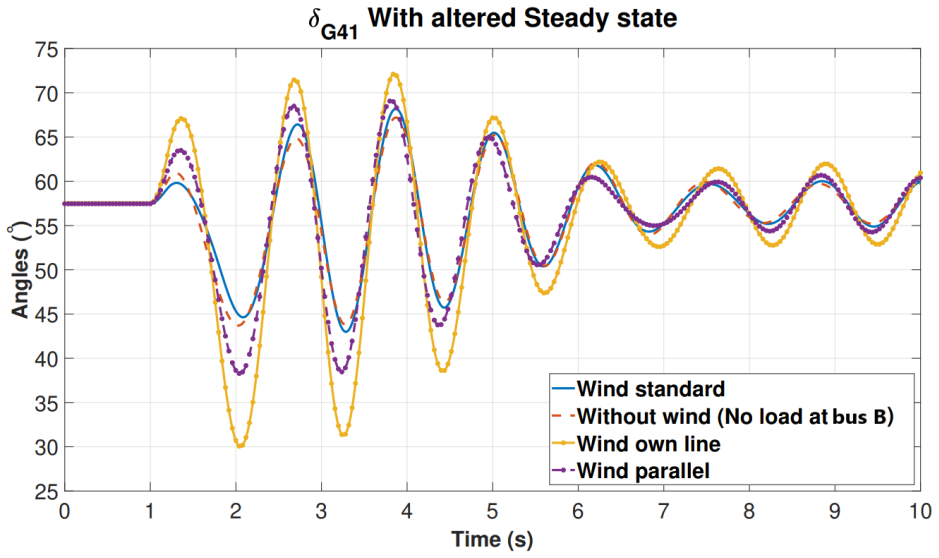

Figure 6.32: Angle oscillation for G41 when there is a bolted fault at G42 for 200 ms. Angles for the different models are set to match each other before the fault

Here it is found that the smallest oscillation in rotor angle is achieved for the model "Standard". The reason for this can be found if Figure 6.27 is studied, here it is clear that this model manages to keep the voltage highest, so the generator is able to transmit more active power in this case compared to the other cases. This

means that the acceleration of the generator is smaller, so the angle deviation is also smaller. This logic holds for all four cases so the result here is as expected.

So far, for all cases with the WPP connected in this chapter, a strong fault current injection from the WPP has been used if nothing else stated. Now a comparison will be made to see if the voltages at G41 are held at the same levels or not if the fault current injection from the WPP is removed. A 200 ms bolted fault at G42 is once again applied and the resulting voltages at G41 can be found in Figure 6.33.

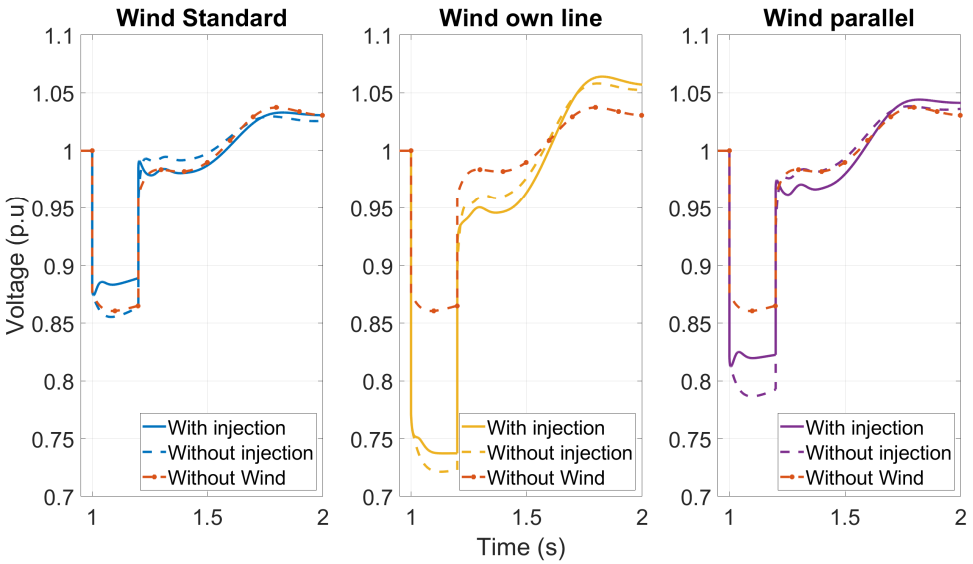

Figure 6.33: Voltage at G41 for the different models during a 200 ms bolted fault at G42, with and without fault current injection from the WPP. The case without wind is also included.

From Figure 6.33 it is clear that the fault current injection manages to keep the voltage slightly higher than without it, even though there is a considerable amount of impedance between the WPP and G41 in all cases. How much the injection raises the voltage will depend on how much impedance there is between the bus connected to the WPP and the bus at G41. For the model "Parallel" the impedance is the lowest since the WPP is connected at 20 % of the two transmission lines connected from Ringhals to bus B.

For the model "Standard" the ability to raise the voltage is slightly smaller since the impedance is slightly higher. In the model "Own line" the ability to help is smallest since the impedance between the two buses is largest. This is also the case where the voltage drops the lowest during the fault, since the two generators G41 and G42 are connected very closely in this case. The expression of the impedances between the WPP and G41 for the different models are shown in Table 6.4. The impedance from the generators and impedance from the WPP converter are omitted from these expression.

Table 6.4: The impedance between the WPP and G41 for the different models.

Model	Total impedance (expression)
Standard	$Z_{Twind} + 1.8 \cdot Z_{line} + Z_{T41}$
Own line	$Z_{Twind} + 2 \cdot Z_{line} + Z_{T41}$
Parallel	$Z_{Twind} + 0.2 \cdot Z_{line} + Z_{T41}$

6.6 Impact on critical fault clearing times from wind power plant

As mentioned in section 6.2, one of the ways of verifying the model used in this project was to put a 3-phase fault at bus B and check the CFCT at Ringhals. In this section, the WPPs impact on this will be investigated.

6.6.1 Accounting for stability changes in the model

Adding a WPP to the model introduces new generation to the system which changes the loading of the lines, which in turn changes their reactive power consumption. At the same time, the WPP also has its own reactive power consumption due to its step-up transformer. Both these factors impact how much reactive power Ringhals must produce. It is not known how a future WPP would take responsibility of supplying the grid with reactive power, i.e., what control modes will be used. The grid codes only specify the required reactive power capability of the WPP, as written in section 2.3.2. Due to the configuration of the WPP and Ringhals in PSS/E, Ringhals generators produce most of the reactive power during steady state and the WPP produces less. This is likely an effect of larger internal impedance of the WPP and its transformer compared to the generators at Ringhals. This causes a problem since the reactive power production and the voltage at Ringhals are key factors when it comes to CFCT. Ideally, both voltage and reactive power can be kept at the same values for the models both with and without WPP to make a fair comparison between different models.

For a load flow in the model without the WPP, both generators G41 and G42 produce almost exactly 150 MVar. When the WPP (with V-control) is added to the model the reactive power output from Ringhals will increase slightly even if the active power production from the WPP is low, due to reasons explained in the previous paragraph. If the active power production from the WPP is increased to its maximum the reactive power production from Ringhals will increase further, so the rotor angle will increase at the same time as the load angle increases due to more active power being transmitted over the line.

To compensate for this the reactive power production from G41 and G42 was locked at 150 MVar for both the case with low wind production (20 MW) and the case with high production (1500 MW). This will of course lower the voltage at Ringhals,

which is not acceptable if the same operating point is supposed to be achieved. One solution could be to force the WPP to produce more reactive power, but this was complicated due to the difference in impedance between WPP and G41 and WPP and G42. Instead, the chosen solution was to place one load each at the two generator buses and have them produce a small amount of reactive power so that the voltage could be kept at the correct values at the same time as the initial reactive power production could be kept at the same magnitude. This value was chosen as the difference between the amount of reactive power production called for by PSS/E in the case with and without the WPP. This kept the voltage at 1 p.u at the buses and a production of 150 MVar, which meant that the reactive power injection from the load was larger for the case with larger active power production from the WPP. When the fault was applied the negative loads were disconnected simultaneously so that they would not interfere with the dynamical simulation.

6.6.2 Resulting critical fault clearing times

The different cases that were simulated are:

- "Fault current injection": The WPP stays connected both during and after the fault and injects a reactive fault current.
- "No Fault current injection": The WPP stays connected both during and after fault but does not inject any fault current.
- "WPP tripped": The WPP trips at the same time as the fault occurs and does not connect to the grid when the fault is removed.

The resulting CFCTs when a bolted fault was applied at bus B for these three cases, are shown in Table 6.5 below.

Table 6.5: CFCTs for the "Standard" model with some different behavior from the WPP.

Case	Low wind (ms)	High wind (ms)
Fault current injection	262	259
No fault current injection	260	257
WPP tripped	254	240

The results are expected since the table shows that the CFCTs decrease when the WPP contributes less to upholding the voltage. It is also expected that increasing the active power production from the WPP would further decrease the CFCT, since a higher loading of the lines increases the angles at Ringhals. It was also noticed that G41 tripped first for all cases since it is connected further away from the WPP so it cannot help it in the same way as it can for G42 (For model standard that

is, for other models the case is different). How the times would vary if G41 was disconnected was also evaluated. In these cases, G42 is the generator that loses synchronism instead. Results are below in Table 6.6 for the "Standard" model, in Table 6.7 for the "Parallel" model and finally in Table 6.8 for the "Own line" model. Today, the CFCT for Ringhals G41 is about 270 ms, for a connection where G41 and G42 shares one transmission line, the CFCT is decreased with about 20-30 ms.

Table 6.6: CFCTs for the "Standard" model with some different behavior from the WPP. G41 has been disconnected.

Case	**Low wind (ms)**	**High wind (ms)**
Fault current injection	278	274
No fault current injection	270	266
WPP tripped	263	245

Table 6.7: CFCTs for the "Parallel" model with some different behavior from the WPP.

Case	**Low wind (ms)**	**High wind (ms)**
Fault current injection	265 ms	262 ms
No fault current injection	261 ms	259 ms
WPP tripped	253 ms	241 ms

Table 6.8: CFCTs for the "Own line" model with some different behavior from the WPP.

Case	**Low wind (ms)**	**High wind (ms)**
Fault current injection	252 ms	252 ms
No fault current injection	252 ms	250 ms
WPP tripped	247 ms	238 ms

For Table 6.6, in all cases, the load at bus B is changed in the same way as in section 6.5 to make sure that the equivalent generator does not start transferring active power, which would cause the angle at bus B to become negative. This is done to keep the equivalent generator in a similar load point for all cases, so that it affects

the results minimally. Changing the load at bus B might not be a completely realistic way of managing the simulation, but it was deemed a better alternative than letting the angle at bus B be negative. When looking at angles in a power system, a large generator that always has the angle zero is not a fully accurate stand-in but is sufficient in this case.

If a comparison is made between Table 6.5 and 6.7 the cases "Fault current injection" and "No fault current injection" are slightly higher for the "Parallel" model. This is expected since, for the "Standard" model, it was G41 that lost synchronism in those cases. In the parallel model the impedance between WPP and G41 is lower so the WPP can impact the voltage at G41 and help increase its CFCT slightly. For the "WPP tripped" case there is no noticeable difference. If instead Table 6.5 and 6.7 are contrasted with Table 6.8, all cases in Table 6.8 have somewhat lower values. It can also be noted that all cases have almost the same values. This is caused by the configuration of the grid, where the WPP has no way of injecting any fault current that can reach G41 or G42 since there is a bolted fault between them. The "Own line" model is also, as has been shown before, the model with the largest impedance between generators G41 and G42 which limits its ability to help raise the voltage quickly after a fault has been cleared.

6.6.3 Analysis of result

To further compare and clarify what difference a high or low active power production from the WPP does, the rotor angle for generator G42 has been plotted for two cases in Figure 6.34. To make the comparison fair, a fault with the same duration as the CFCT of the 1500 MW case has been applied for both a 20 MW and 1500 MW case. Fault current injection from the WPP is used for both cases. The "Standard" model has been used.

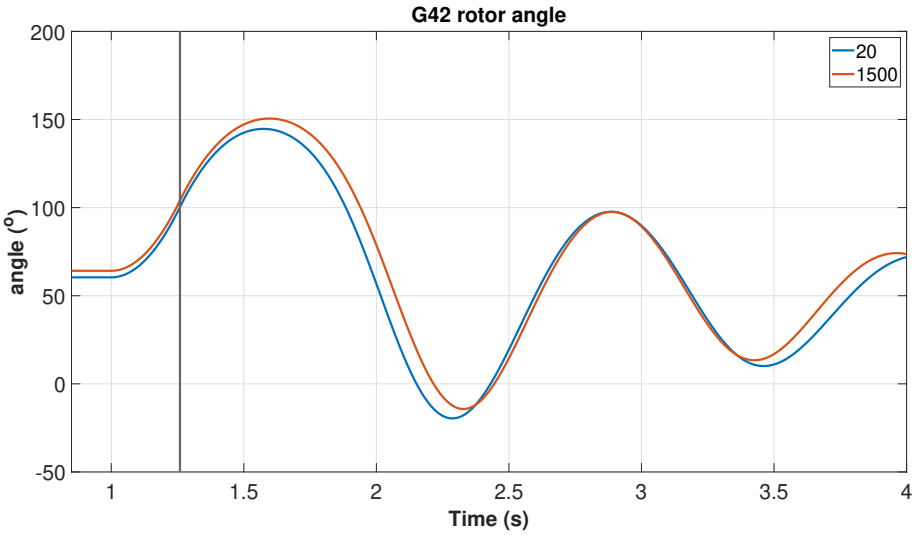

Figure 6.34: The rotor angle for G42 for the two different cases. The grey vertical line shows where the fault is cleared.

The graph shows clearly that the angles increase for a while after the fault has been cleared, which is what is expected if the equal area criterion (EAC) is considered. However, EAC states that the highest possible angle for a generator that remains stable during a fault event is 180° - $\delta_{steady-state}$, which would clearly be a smaller value (circa 120 °) than the maximum for both cases in Figure 6.34, which is almost 150°. This can seem strange since this is the theoretical limit if it is assumed that the generator returns to the same P-δ curve as before the fault.

What this assumption means is that both the back EMF, E, and the terminal voltage, V_T, returns to 1 p.u almost instantaneously after the fault. However, the generators at Ringhals are equipped with AVRs that increase the field current which leads to an increase in back EMF after the fault, so it is not likely that the previously stated assumption holds and it is not reasonable to assume that the generator will return to the same P-δ curve as soon as the fault is cleared. To study the increased back EMF it is necessary to first look at the field current in the generator and then calculate the resulting back EMF via the saturation curve of the PSS/E model for a round rotor SG. Figure 6.35 shows a generic saturation curve used in the program.

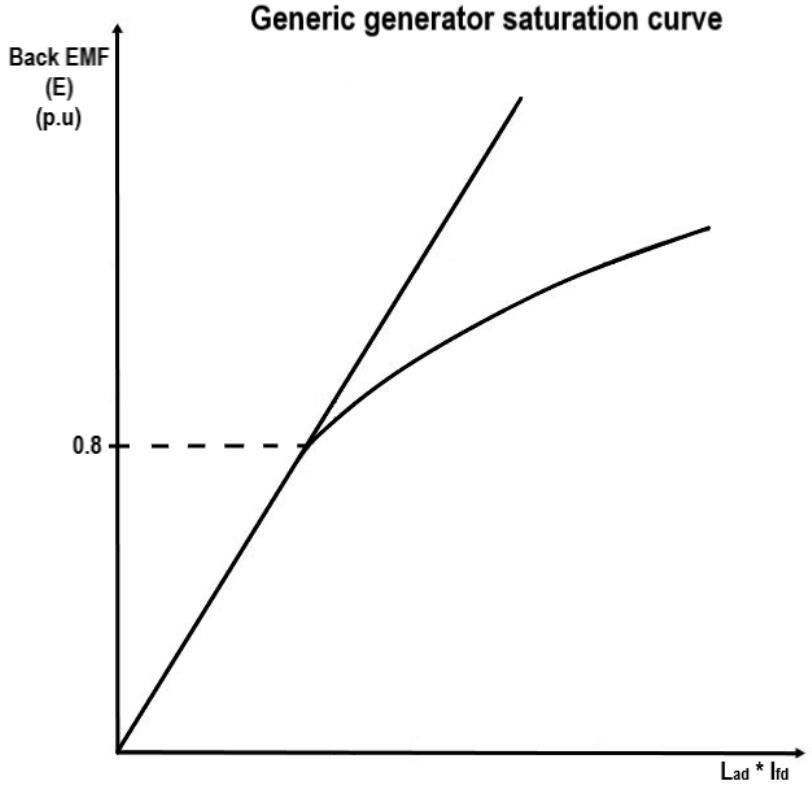

Figure 6.35: Generic generator saturation curve. The tapered lines represent the Back EMF when the generators is saturated.

If the straight line in Figure 6.35 is considered, the back EMF would be equal to field current in per unit base. This is not the case in an actual generator because of saturation effects that occur when the current is above a certain value. For a model

to be somewhat realistic this needs to be accounted for, which is the case for the curve which tapers off. For the generator models used in this project, the saturation starts at approximately 0.8 p.u of field current. How much the curve tapers is decided by a set of two constants that are varied for different generators. These constants were used to calculate the particular tapered curve for the generators used in the simulation. Then the value of field current was compared with the point at which saturation starts, 0.8. If the field current was higher the back EMF was fit to the tapered curve instead of the line. Both the injected field current and the resulting back EMF for one case is shown in Figure 6.36.

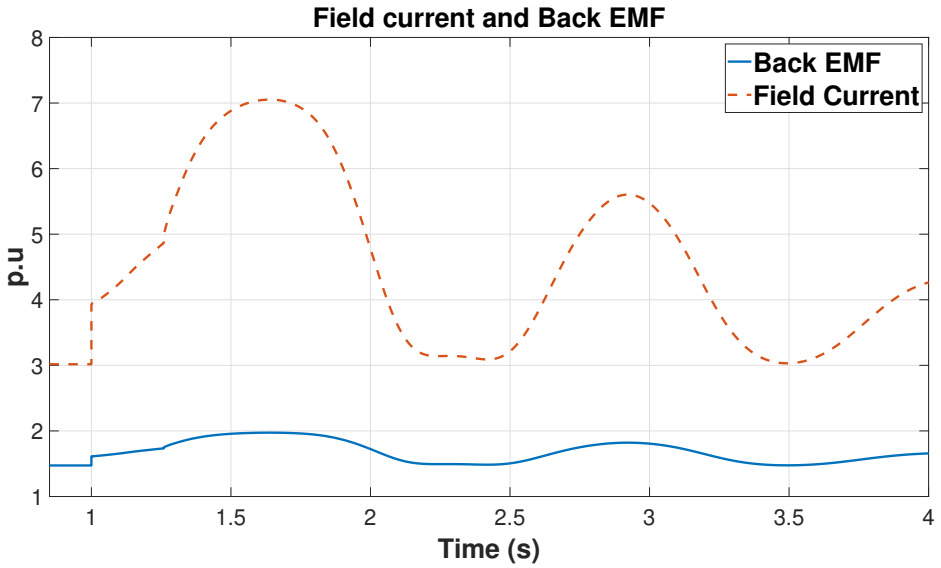

Figure 6.36: Field current injected by the AVR and the resulting back EMF. This is for the 20 MW case.

It is clear that the AVR is very strong since the injected current has a peak of about 7 p.u. This means that the generator will be heavily saturated, and will only reach a back EMF of 2 p.u. This clearly illustrates that the generator will not return to the pre-fault P-δ curve once the fault is cleared.

One way of showing the difference between the 20 MW and 1500 MW scenario is to plot the product of the generators terminal voltage, V_T, The back EMF E and sine of the rotor angle δ to visualize the whole picture, as seen in Figure 6.37.

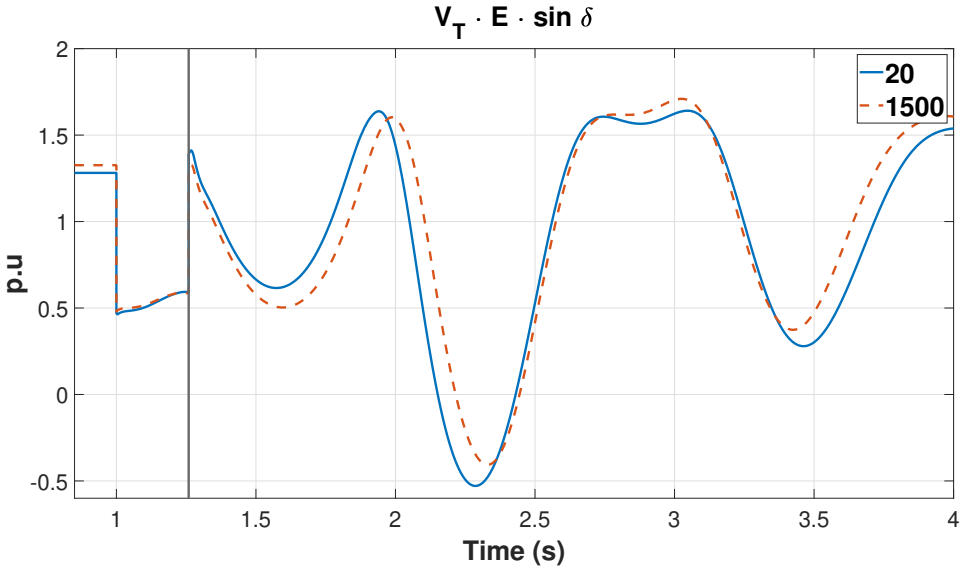

Figure 6.37: The product of $V_T \cdot \mathrm{E} \cdot \sin(\delta)$ for both production scenarios.

The equation for active power transmitted by a generator is

$$P = \frac{E \cdot V_T}{X} \cdot sin(\delta) \tag{6.14}$$

where X is the impedance from the sending end to the receiving end. The only parameter from the equation that is not used in Figure 6.37 is the impedance, which should be identical for both cases and thus would only influence the scaling of the y-axis. One way of expressing it is to say that X is assumed to be 1 p.u in both cases.

In the simulations where the generator lost synchronism, it would happen soon after the fault was cleared. As can be seen in Figure 6.37, the 20 MW scenario has a slightly higher amplitude in the time window of fault clearance and two seconds, this keeps the generator from losing synchronism. After two seconds the curve starts oscillating in such a manner that the amplitude actually becomes negative for a brief period. During this period, the rotor angle is negative, which can be seen in Figure 6.34. To make the situation as clear as possible the resulting P-δ curves for the 20 MW production scenario has been plotted in Figure 6.38

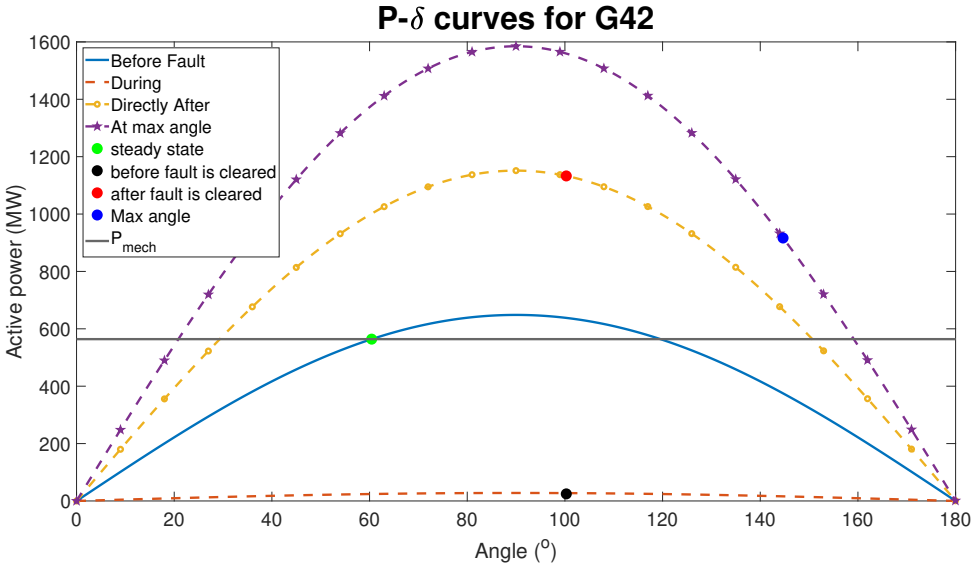

Figure 6.38: P-δ curves for G42 before, during, and after a fault of duration 259 ms.

First, the method used for plotting the P-δ curves needs some explaining. The first step is to take the active power output at a certain point and divide it by sine of the rotor angle at the same point. This equals the expression $\frac{E \cdot V_T}{X}$ from 6.14 and will be the peak amplitude of the plot. This enables plotting of the P-δ-curve without knowledge of the impedance of the system. $\frac{E \cdot V_T}{X}$ is simply the amplitude and is plotted times sine of delta against delta for the interval 0-180 degrees.

When the generator is operating in steady state it will follow the blue curve in the graph. For the used load and grid configuration the green dot signifies the steady state angle. When the fault occurs the generator drops to the red line that is barely above the x-axis. The drop is from 654 MW down to approximately 20 MW. Since P_{mech} is still at the same value, the generator will start to accelerate, and the angle will increase. The black dot shows the maximum value that the angle reaches right before the fault is cleared at 1.259s. When the fault is cleared the generator jumps up to the red dot on the yellow curve. In a theoretical description of the EAC the generator starts to slow down here since $P_{elec} > P_{mech}$, although the angle will keep increasing until rated speed is reached. This is true in this case but with the significant difference that the generator angle will not move towards its maximum value along the yellow curve. Instead, the back EMF will continue to increase further, as can be seen in Figure 6.36, and the amplitude of the $P - \delta$ curve will therefore increase to the purple star-dashed line. The blue dot is the maximum value of the angle for this fault. The generator reaches the blue dot at 1.573 s into the simulation. As is obvious from Figure 6.38, the machine would have lost synchronism in this case if the active power were not increased dramatically after the fault was cleared.

6.7 Fault currents

As was mentioned before, one concern regarding where the WPP will be connected is that certain connections could increase the fault current at Ringhals in a way that could potentially damage equipment at Ringhals. For the model "Standard" as shown in Figure 6.1, the fault currents are listed in Table 6.9. For the models "Parallel" and "Own line", the fault currents are listed in Table 6.10 and 6.11 respectively. The maximum fault currents were obtained through PSS/E, it was controlled so that the fault current from the WPP was 1.2 p.u of rated current at the wind bus, before the 400 kV transformer.

Table 6.9: Maximum fault currents for "Standard" model with saturated subtransient impedance, with and without WPP.

Bus	With WPP (kA)	Without WPP (kA)	Deviation (%)
G32	148.1	147.7	+0.27
G42	156.5	153.4	+2.02
T42	16.91	15.47	+9.31
B	29.62	28.12	+5.33
A	25.36	24.74	+2.51

Table 6.10: Maximum fault currents for "Parallel" model with saturated subtransient impedance, compared to standard model without WPP.

Bus	With WPP (kA)	Deviation from original without WPP (%)
G32	148.1	+0.27
G42	163.0	+6.26
T42	20.93	+35.29
B	29.67	+5.51
A	25.38	+2.59

Table 6.11: Maximum fault currents for "Own line" model with saturated subtransient impedance, compared to standard model without WPP.

Bus	With WPP (kA)	Deviation from original without WPP (%)
G32	148.0	+0.20
G42	157.6	+2.74
T42	17.62	+13.90
B	29.52	+4.98
A	25.32	+2.34

From the above tables, it can be noted that all models and buses would experience a higher fault current, given that the WPP has fault current injection. The

most severe increase is for the Parallel model at bus T42, this is because the fault current contribution is increased from both bus B, G41 and from the contribution from the WPP. This large increase is considered as a major drawback to this connection alternative, as a fault current this high could damage electrical equipment at Ringhals.

6.8 Conclusion from simulations

What can be concluded from the simulations in this chapter is that if a WPP is to connect to the transmission lines currently utilized by Ringhals, it could have a considerable impact on the voltage magnitude during a fault and will also impact the CFCT. This will be dependent on how the Swedish grid codes changes in the future and what demand SvK sets on the WPP when it comes to fault current injection. Furthermore, the maximum fault currents near Ringhals could increase to a certain extent, given that the WPP will be required to provide fault current injection. When it is decided how the WPP will connect to the 400 kV grid and more is known about its rated power, new simulations regarding all of the explored phenomena in this report are needed to draw more detailed conclusions.

The simulations have also shown that if the WPP is connected so that it shares a transmission line with a generator at Ringhals it can help increase its voltage during an external fault in a significant way, which can increase its CFCT. If instead the WPP ends up connecting to both lines it can help both generators to a lesser degree, meaning that the overall CFCT will be slightly shorter when compared with the case where the WPP shares a transmission line with a generator and one generator is down for maintenance. For the case where the WPP is appointed its own transmission line and G41 and G42 share one transmission line the WPP will be most limited when it comes to impacting the voltage at either of these generators. This decreases the CFCT for the two generators since the transmission line they share will be more heavily loaded resulting in a higher rotor angle, decreasing the CFCT with about 20-30 ms. This connection might still be looked upon favorably if other factors, such as harmonics or SSO is seen as an issue, since it has slightly higher impedance between Ringhals generators and the WPP than the other cases. Finally the connection alternative "Parallel" would result in a very large increase of fault current, which could damage electrical equipment at Ringhals.

7

Inter-area Oscillations

Inter-area oscillations are identified as low-frequency oscillations where weakly coupled SGs swing against each other. The oscillations can pose a serious threat to any power system. In this chapter, inter-area oscillations and their connection to type 4 WPP will be explored.

7.0.1 Theoretical description of inter-area oscillations

In [40] a comparison is made between systems of masses connected via springs and SGs connected in a power system. In the simplest case, we can consider a mass-spring-damper system and a single SG connected to an infinite bus, called a single machine infinite bus. For the spring, the second-order differential equation is

$$\ddot{x} + \frac{b}{m} \cdot \dot{x} + \frac{k}{m} \cdot x = 0 \tag{7.1}$$

where x is displacement, m is the mass, b is the damping coefficient and k is the spring constant. The swing equation for the SG can be written as

$$\frac{d\omega}{dt} = \frac{(T_m - T_e(\delta) - K_d\omega)}{2H} \tag{7.2}$$

where ω is the SGs angular velocity, T_m is the mechanical torque applied to the generators turbine, T_e is the electrical torque produced by the generator, δ is the rotor angle of the SG, K_d is the damping coefficient, and H is the inertia constant of the SG. Since $\frac{d\delta}{dt} = \omega$ linearization of the swing equation around angle $\delta = \delta_0$ can be done to get the equation

$$\Delta\ddot{\delta} + \frac{K_D}{2H}\Delta\dot{\delta} + \frac{K_s\omega_0}{2H}\Delta\delta = \frac{\omega_0}{2H}\Delta T_m \tag{7.3}$$

The mass-spring system and the single machine infinite bus resemble each other in terms of differential equations, natural frequencies, and damping ratios. The mass corresponds to the machine inertia and the spring constant corresponds to the synchronizing power coefficient, which is inversely proportional to the line reactance X_T and more precisely described by

$$K_s = \frac{V_T E}{X_T} cos\delta_0 \tag{7.4}$$

where V_T and E is the terminal voltage and back EMF respectively. Since the two differential equations are similar, their natural frequencies (ω_n) and damping (ζ) are also calculated in a very similar way, as

$$\omega_n = \sqrt{\frac{k}{m}}, \zeta = \frac{b}{2m\omega_n} \tag{7.5}$$

for the spring, and as

$$\omega_n = \sqrt{\frac{K_S\omega_0}{2H}}, \zeta = \frac{1}{2}\frac{K_D}{2H\omega_n} \tag{7.6}$$

for the SG. If the same type of comparison is made between a system with two masses connected by a single spring and two generators connected by a transmission line it will result in two different swing equations, as

$$\Delta\dot{\omega}_1 = \frac{1}{2H_1}(\Delta T_{1m} - \Delta T_{1e} - K_{D1}\Delta\omega_1) \tag{7.7}$$

for the first generator, and as

$$\Delta\dot{\omega}_1 = \frac{1}{2H_2}(\Delta T_{2m} - \Delta T_{2e} - K_{D2}\Delta\omega_2) \tag{7.8}$$

for the second generator. If linearization is done in the same way as before, the system can be represented in state space form with the following matrix

$$\begin{pmatrix} \Delta\ddot{\delta}_1 \\ \Delta\ddot{\delta}_2 \end{pmatrix} = \begin{pmatrix} \frac{-K_{11}}{2H_1} & \frac{-K_{12}}{2H_1} \\ \frac{-K_{21}}{2H_2} & \frac{-K_{22}}{2H_2} \end{pmatrix} \begin{pmatrix} \Delta\delta_1 \\ \Delta\delta_2 \end{pmatrix} \tag{7.9}$$

from this matrix it is possible to derive an expression for the natural frequency as

$$\omega_n = \sqrt{\frac{K_{11}}{2H_1} + \frac{K_{22}}{2H_2}} \cdot \omega_0 \tag{7.10}$$

and if both generators are seen as areas this frequency is the inter-area frequency. The generators will oscillate with this frequency completely out of phase from each other unless this oscillation is damped. An area is defined by generators that are strongly connected, meaning that the impedance between the generators is low. When considering generators as being in different areas the impedance between them is high so the coupling is weak.

According to [41] the two most critical inter-area modes in the Nordic system are at 0.29 Hz and 0.55 Hz where the first mode is between Finnish generators and the other generators in the system. The 0.55 Hz mode is between generators in the north of Norway, Sweden, and Finland and the southern parts of all three countries. These oscillations must be damped so that they do not increase in amplitude and cause generators to lose synchronism. The most common way of doing this is with PSSs.

7.0.2 Type 4 wind power plants and oscillations in the grid

In [42], the impact of Type 4 WPPs on inter-area modes of oscillation is evaluated in a grid model and it is found that the WPP does not seem to interact with the inter-area modes of the system. This is because of the full converter design where the permanent magnet synchronous generator (PMSG) used in the WTs is isolated from the grid. Therefore, mechanical oscillations from the WT cannot reach the grid. Also, converters do not interact with oscillations in the same way as SGs since a converter does not have moving parts. One thing that differentiates the case evaluated in said article is that the authors replaced SGs with WTs, whereas no synchronous production is being removed in the case studied in this report. It is only CBG that is being added, which could potentially lead to a different result.

In [43] it is concluded that Type 4 WTs do not interact with SGs through inter-area modes, however, new electromechanical modes are introduced by the WTs. In the article, this is found by taking a grid model with SGs and replacing some of them with Type 4 WTs until all the SGs have been replaced. Whenever an SG is replaced two electromechanical modes associated with that generator are removed but two new modes associated with the WT are added. One mode is associated with most other Type 4 WTs in the system and has a lower damping, the other one has higher damping and is associated only with a few of the WTs. In [43] these new modes are called "strong interaction modes" and "weak interaction modes" respectively and they are dominated by the mechanical state variables of the WTs.

No clear law regarding their increased or decreased damping is found so some modes experience increased damping with increased WT penetration of the system, but some have decreased damping with increased penetration. Important to note however is that none of the modes are critically underdamped before wind penetration of the grid becomes remarkably high (>80%). This will not be the case for the Swedish transmission grid in the near future but beyond that one can only speculate. It is important to consider that [43] sees a system with SGs being replaced with WTs, not WPP consisting of several interconnected WTs. If the phenomena with strong and weak interaction modes exist in the case with increased WPP integration is not known at this time but it can be seen as a risk.

Another thing that is worth considering is that in [44] it is found that a Type 4 WPP can effectively contribute to the damping of low frequency oscillations in the power system. This will be explored later in this chapter.

7.1 Damping of inter-area oscillations

Since inter-area oscillations affect the rotor of a generator traditionally they are damped by a PSS connected to the generator. The PSS is briefly described in chapter 2.

7.1.1 Damping from Type 4 wind power plants

In [45] it is briefly mentioned that a WPP consisting of Type 4 WTs can be used as power oscillation damping (POD) controllers. This is expanded upon in many articles. Before this concept is described it is worth noting that the feasibility of its construction will depend on if SvK makes specific demands of this type of functionality or if Ringhals can show that the situation in the grid has gotten worse after the introduction of a WPP. In [46], the authors investigate damping of system oscillations after a bus fault with the use of a power controller, which controls both active and reactive power. Such a controller would be added to the existing controller, regulating active and reactive power. Normally this type of controller is used to keep the WPP operating in maximum power point tracking operation, but its references can be augmented to use some of its capacity to damp oscillations. For the reactive power controller an equation is created using the angular velocity, ω, of the nearest SG, which would be one of Ringhals generators in this case and is written as

$$\Delta Q = \omega \cdot G \cdot \frac{sT_{w1}}{1 + sT_{w1}} \tag{7.11}$$

where G is the gain and T_{w1} is the time constant of the washout filter used for removing the steady state component of the signal. The authors of [46] also adds that some delay compensation will most likely be needed in the controller due to the inertia of large SGs, although this is left out of this simplified description. Figure 7.1 below shows the generic reactive power controller for a WPP with this new equation added, as described in [46].

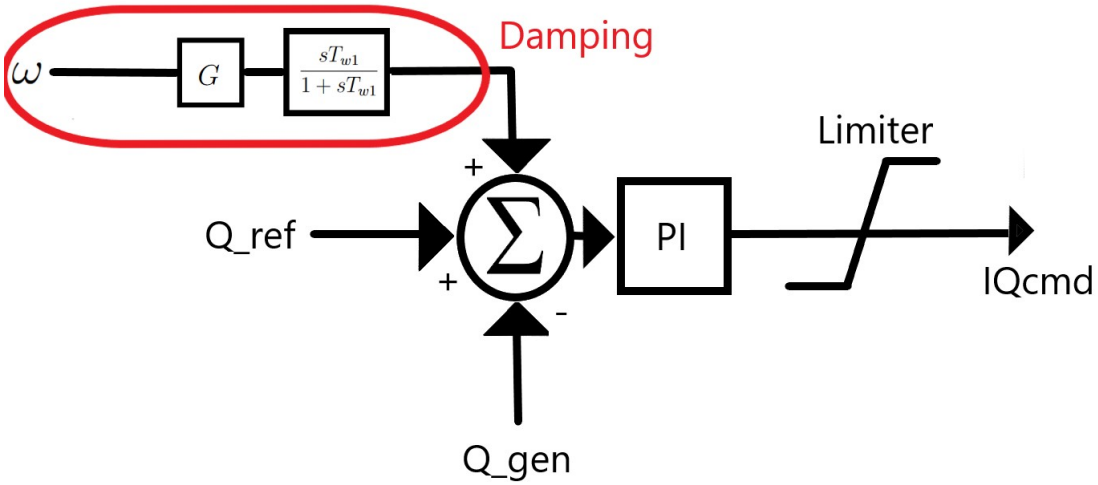

Figure 7.1: Generic reactive power controller for a WPP with added damping.

For the active power part of the controller, the angle δ at the PCC is used as input in the equation

$$\Delta P = \delta \cdot G \cdot \frac{sT_{w1}}{1 + sT_{w1}} \tag{7.12}$$

Delay compensation is also left out here even though it is necessary for a successful implementation. The signal is then fed into a similar controller to the ones used for reactive power control, as can be seen in Figure 7.2.

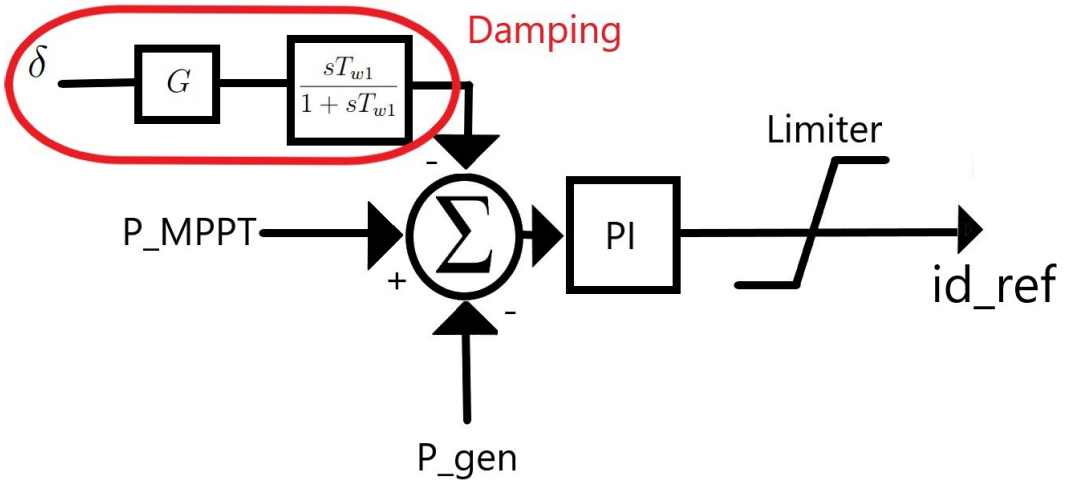

Figure 7.2: Generic active power controller for a WPP with added damping.

The controllers are similar, but it is important to note the signs at the summation block for the damping signal in the two different cases. For the reactive power controller, it is positive since the goal is to boost the reactive power output to help maintain the system voltage. For the active power case it is negative so that the active power output is limited when the angle increases. It is important to note here that these diagrams are simplifications and are not meant to be completely accurate, they are only meant to illustrate the concept of incorporating POD into the controllers. The actual controller is much more complicated with many more blocks.

In [46], both controllers are evaluated separately but also combined. The reactive power POD is the slowest, active power POD is slightly faster, and combined POD is the fastest. In the cases using active power for POD the output from the WPP is kept low before the fault so that there is headroom for damping. Limiting the output will of course be very costly for the operator of the WPP and is it not likely that it will happen unless it is required by SvK, which currently is not the case.

For this type of oscillation damping to be possible, coordination must be done with the closest SG, which would be one at Ringhals. The WPP POD controller would then need to use the angular velocity of a Ringhals generator as input. Of course, it would first need to be established if such sharing of information from Ringhals is possible. The next step would most likely be to decide how that information will be sent and investigate how large the delay would be for the information to arrive at the WPP.

In [47] it is described how FACTS devices such as STATCOMS can be utilized for damping of power oscillations at the PCC for a WPP. It is mentioned that for many

cases it might be better to use a STATCOM for reactive power injection instead of relying on the WPP since it consists of many turbines and the control of these are more complicated than controlling one STATCOM. It is also mentioned that most projects studying the reactive power control from WPP overlook this aspect since all WTs are aggregated into one unit.

Since any damping contributed by a Type 4 WPP will be dependent on complex control systems and power electronics, an installation like any of the examples mentioned in this chapter will introduce the risk that one of these systems would malfunction or be improperly tuned. This can lead to undesirable behaviors, since if the WPP has the ability to dampen oscillations, it must also have the ability to amplify oscillations.

7.2 Conclusions

According to most sources, a Type 4 WPP will not interact with inter-area modes. However, according to [43] there is a risk that new modes of oscillation that are strongly associated with the mechanical states of the WTs in the WPP are introduced into the system. Since the damping of these does not follow a predictable law, a detailed analysis of the needs of damping for these modes can become necessary.

On a final note, if it is decided that the WPP needs to contribute to damping of oscillations in the grid, some amount of coordination with Ringhals might become necessary. Partly to make sure that the damping at the WPP is functioning and that it does not compete with the damping supplied by Ringhals. Adding damping capabilities also means adding layers of complexity to the controller at the WPP which could increase the risk of faults.

8

Conclusion

The purpose of this report was to determine and investigate possible effects that Ringhals power plant could experience in the case of an adjacent connection of an offshore WPP. This was conducted through a literature review, indicating special phenomena inherent to a WPP, and though simulations, indicating behavior under abnormal dynamic events in the surrounding grid.

It is important to underline that as few technical aspects are determined in the planned WPPs the results found should mainly be interpreted as an expected behavior and could thus change depending on specific components and control schemes. Despite its limitations, the study certainly adds to our understanding of implications that a Type 4 WPP poses to an adjacent thermal power plant where the key conclusions that can be drawn from the result are:

- Harmonic emission from a Type 4 WPP should not be of major concern, given proper filter techniques and that regulations are followed.

- If a connection alternative is chosen where the WPP is connected electrically close to a Ringhals generator, such as the model 'Standard', the risk of SSO is significant during operation when the grid is significantly weak.

- Inter-area oscillations could become more problematic if a large WPP is connected very close to Ringhals, in this case a POD controller could be installed in the WPP that would limit this negative effect, but it is not clear how the controller would interact with PSSs of Ringhals generators.

- The simulations indicate that the grid, in its current condition should be able to sustain the impact of a sudden trip of a WPP without serious voltage deviations.

- Fault current injection from the WPP increases the CFCT slightly, but if the WPP disconnects from the grid during a fault the decrease in CFCT is major. The fault current injection benefits Ringhals the least in the model 'Wind parallel'.

- For the model "Own line" the decrease in CFCT is 20-30 ms.
- The connection alternative "Parallel" results in a much larger maximum fault current at Ringhals, which could damage equipment.

8.1 Future work

There were other possible phenomena that was deemed necessary to study further, although was not due to limitations, either in information, software, or time. These phenomena are briefly discussed in this section.

To begin with, considering a WPPs nature of intermittent generation, voltage fluctuations in the surrounding grid may follow. This could result in an increased activity of the AVRs at Ringhals, putting more stress to the generators. The control system of the WPP should be investigated to find risks for unforeseen conflicts with Ringhals control system.

Another thing that is important to remember is that all conclusions drawn in this project may change in the future if regulations or the layout of the grid or both are subject to change. The Swedish electricity system is facing many changes which are important to keep track of in the future in order to properly protect Ringhals. As of now there are not many, if any, cases alike what is planned in the surrounding grid of Ringhals, i.e, large Type 4 WPP electrically close to a nuclear power plant. It is therefore important to keep updated on information and reports of similar installations once available.

Furthermore, this report does not cover any implications that the WPP might cause on different protection equipment at Ringhals, such as relays. As can be seen in Table 6.9, the fault currents at bus G32 and G42 does not change much with the addition of a WPP with fault current injection capabilities. Although it is unclear how large portion of the fault current originates from the WPP, and what the realistic maximum portion would be. This could potentially be an important aspect to consider, as the characteristics of fault current from CBG is different when compared to an SG. In particular, the amplitude of negative-sequence fault current is very low [48]. Coordination of protection systems between Ringhals and future WPPs might become necessary.

At the start of this study, it was believed that only one of the planned offshore WPPs would be approved to connect near Ringhals, recently though, two offshore WPPs have been granted approval with the suggestion to connect in the immediate vicinity of Ringhals. Only one of these WPP will have a large enough capacity to connect directly to the transmission grid so it is not known how the connection of the other WPP to a lower voltage grid might impact Ringhals. A new study might be necessary once more is known about how the smaller WPP will connect to the grid to understand if the two WPPs might interact with each other and what implications this might have on Ringhals.

Bibliography

[1] "IEEE Recommended Practice and Requirements for Harmonic Control in Electric Power Systems," *IEEE Std. 519-2014*, 2014. (Accessed 2023-03-31) https://ieeexplore.ieee.org/stamp/stamp.jsp?tp=&arnumber=6826459.

[2] "SS-EN 50160 Spänningens egenskaper i elnät för allmän distribution," *SEK Svensk Elstandard*. (Accessed 2023-05-23) https://www.sis.se/api/document/get/80020782.

[3] "Fortsatt hög elproduktion och elexport under 2021 — energimyndigheten.se." (Accessed 2023-01-16) https://www.energimyndigheten.se/nyhetsarkiv/2022/fortsatt-hog-elproduktion-och-elexport-under-2021.

[4] "Långsiktigt marknadsanalys 2021," *Svenska kraftnät*, 05 2021. (Accessed 2023-01-16) https://www.svk.se/siteassets/om-oss/rapporter/2021/langsiktig-marknadsanalys-2021.pdf.

[5] Regeringen, "Mål för energipolitiken," 05 2021. (Accessed:2023-01-16) https://www.regeringen.se/regeringens-politik/energi/mal-och-visioner-for-energi/.

[6] Jonas Fagerström, "Politikerna positiva men medborgarna skeptiska – rekordlåg andel vindkraftverk beviljades förra året," *Aktuell Hållbarhet*, 2022. (Accessed 2023-01-19) https://www.aktuellhallbarhet.se/miljo/energi/politikerna-positiva-men-medborgarna-skeptiska-rekordlag-andel-vindkraftverk-beviljades-forra-aret.

[7] Uniper, "Kärnkraft i sverige," 05 2021. (Accessed 2023-01-18) https://www.uniper.energy/sv/sverige/om-uniperi-sverige/karnkrafti-sverige?gclid=Cj0KCQiAiJSeBhCCARIsAHnAzT_XHtKuv6cy7n0LO3QAgrcueP7AtJQOn1MGIAmus7lDBAzoHYXzxQaAnSvEALw_wcB.

[8] "Kattegatt syd samrådsunderlag," *Vattenfall Vindkraft AB, Vattenfall Vindnät Sverige AB*, 01 2021. (Accessed: 02-02-2023) https://group.vattenfall.com/se/siteassets/sverige/var-verksamhet/vindprojekt/kattegatt-syd/su_final_ver_2021-01-05_00.pdf.

[9] "Anslutning av havsvindpark galatea-galene," *OX2*, 2022. (Accessed 2023-04-20) https://www.ox2.com/files/Project_documentation/galatea-galene/Samradsunderlag_anslutning.pdf.

[10] VindkraftFalkenberg, "Om vindpark falkenberg," 05 2021. (Accessed 2023-04-20) https://www.vindparkfalkenberg.se/om-vindpark-falkenberg/.

[11] "De havsbaserade vindkraftsparkerna galene och kattegatt syd beviljas tillstånd," *Regeringskansliet*, 05 2023. (Accessed 2023-05-24) https://www.regeringen.se/pressmeddelanden/2023/05/de-havsbaserade-vindkraftsparkerna-galene-och-kattegatt-syd-beviljas-tillstand/.

[12] Hadi Saadat, *Power System Analysis*. Virginia, USA: PSA publishing, 2 ed., 1999.

[13] Magnus Lenasson, Simon Rohlén, "Effective voltage control and operational coordination of regional reactive power resources," *Energiforsk*, 09 2020. (Accessed 19-04-2023) https://energiforsk.se/media/28395/effective-voltage-control-and-operational-coordination-energiforskrapport-2020-692.pdf.

[14] Prabha Kundur, *Power System Stability and Control*. Palo Alto, California: Mcgraw-Hill, 2 ed., 1994.

[15] E. Energy, "Variable speed turbine with full-rated power converter." (Accessed 02-02-2023) https://www.esig.energy/wiki-main-page/variable-speed-turbine-with-full-rated-power-converter/.

[16] Lena Max, Andreas Petersson, Pehr Hjalmarsson, "Sub-synchronous oscillations between fpc wind farms, vsc-hvdc links and nuclear power plants," 12 2020. (Accessed 19-01-2023) https://energiforsk.se/media/28852/sub-synchronous-oscillations-energiforskrapport-2020-707.pdf.

[17] "Guide för anslutning av kraftproduktionsmodul till överföringssystemet," *Svenska kraftnät*, 03 2021. (Acessed 2023-04-11) https://www.svk.se/siteassets/1.om-kraftsystemet/legalt-ramverk/eu-lagstiftning/anslutningskoder/guide-anslutning-av-kraftproduktionsmodul-till-overforingssystemet.pdf.

[18] Göran Morén, "Energimarknadsinspektionens författningssamling – energimarknadsinspektionen," 12 2018. (Accessed: 03-02-2023) https://ei.se/download/18.5b0e2a2a176843ef8f5b74/1608639227153/EIFS-om-fastst%C3%A4llande-av-generellt-till%C3%A4mpliga-krav-f%C3%B6r-n%C3%A4tanslutning-av-generatorer-EIFS-2018-2.pdf.

[19] "Kraftparksmodul: Bilaga 1," *Svenska kraftnät*, 01 2022. (Accessed 11-04-2023) https://www.svk.se/siteassets/1.om-kraftsystemet/legalt-ramverk/eu-lagstiftning/anslutningskoder/bilaga-1_projektspecifika-uppgifter-och-krav_kraftparksmoduler.pdf.

[20] Tatiana Salnikova et al., "Survey on vibration impact of flexible operation on npp," *Energiforsk*, 2021. (Accessed 24-05-2023) https://energiforsk.se/media/29825/survey-on-vibration-impact-of-flexible-operation-on-npp-energiforskrapport-2021-774.pdf.

[21] Huakun Liu et al., "Subsynchronous interaction between direct-drive pmsg based wind farms and weak ac networks," 2017. (Accessed 19-04-2023) https://eds.s.ebscohost.com/eds/detail/detail?vid=2&sid=cf3df293-4948-4b0a-aebd-8c29e2f41d54%40redis&bdata=JnNpdGU9ZWRzLWxpdmUmc2NvcGU9c2l0ZQ%3d%3d#AN=edseee.7878693&db=edseee.

[22] "Torsional vibrations in turbomachinery," *Engie laborelec*, 2020. (Accessed 25-05-2023) https://www.laborelec.com/wp-content/uploads/2020/11/ENGIE_Laborelec_FAQ-torsional-vibrations.pdf.

[23] Hassan W. Qazi et al, "Impacts of fault ride through behavior of wind farms on a low inertia system," *IEEE Transactions on Power Systems*, 07 2022. (Accessed 20-04-2023) https://ieeexplore.ieee.org/stamp/stamp.jsp?tp=&arnumber=9120224&tag=1.

[24] Espen Hagstrøm, Ian Norheim and Kjetil Uhlen, "Large-scale wind power integration in norway and impact on damping in the nordic grid," *Wind Energy*, 2005. (Accessed 25-05-2023) https://onlinelibrary.wiley.com/doi/epdf/10.1002/we.168.

[25] Daphne Schwanz, Math Bollen, "Harmonics and wind power," *Energiforsk*, 02 2018. (Accessed 23-02-2023 https://energiforskmedia.blob.core.windows.net/media/24015/harmonics-and-wind-power-energiforskrapport-2018-469.pdf.

[26] Lucia Beloqui Larumbe, Zian Qin, Pavol Bauer, "Introduction to the analysis of harmonics and resonances in large offshore wind power plants," *2018 IEEE 18th International Power Electronics and Motion Control Conference (PEMC)*, 08 2018.

[27] Wilsun Xu,IEEE SMARTGRID Resource Center, "Interconnection of inverter-based resources – power quality aspects." (Accessed 01-03-2023) https://resourcecenter.smartgrid.ieee.org/education/webinar-slides/SGSLW0185.html/.

[28] Lukasz Hubert Kocewiak, "Harmonics in large offshore wind farms," *Aalborg University*, 2012. (Accessed 02-03-2023) https://vbn.aau.dk/ws/portalfiles/portal/316423403/lukasz_kocewiak.pdf.

[29] Urban Axelsson et al., "Propagation of harmonic emission from the turbines through the collection grid to the public grid," *22nd International Conference and Exhibition on Electricity Distribution (CIRED 2013)*, 2013. (Accessed 18-03-2023) https://ieeexplore.ieee.org/document/6683460.

[30] Math Bollen, Kai Yang, Daphne Schwanz, "Harmonic aggregation and amplification in a wind-park," *23rd International Conference on Electricity Distribution (CIRED2015)*, 2015. (Accessed 21-03-2023) https://www.diva-portal.se/smash/get/diva2:1005801/FULLTEXT01.pdf.

[31] "Interactions between hvdc systems and other connections," *ENTSO-E*, 2018. (Accessed 10-04-2023) https://eepublicdownloads.entsoe.eu/clean-documents/Network%20codes%20documents/NC%20RfG/IGD-Interactions_between_HVDC_Controllers_final.pdf.

[32] Muhammad Taha Ali, "Analysis of sub-synchronous oscillations in wind power plants," 2020. (Accessed 15-04-2023) "https://www.diva-portal.org/smash/get/diva2:1423448/FULLTEXT01.pdf?fbclid=IwAR111s3SZ8P0aseemfIAEBpDtlaVFXfMk6YjbrFdiju5gvo8y9FSvz0Eckc".

[33] R. J Piwko, E. V. Larsen, "Hvdc system control for damping of subsynchronous oscillations," *IEEE Transactions on Power Apparatus and Systems*, 1982. (Accessed 20-04-2023) https://ieeexplore.ieee.org/document/4111580.

[34] Dharshana Muthumuni, "Sub synchronous oscillations – an introduction," *Manitoba HVDC Research Centre*, 2016. (Accessed 20-04-2023) https://www.pscad.com/knowledge-base/search?module_id=1&q=Sub%20Synchronous%20Oscillations#gsc.tab=0&gsc.q=Sub%20Synchronous%20Oscillations&gsc.page=1.

[35] Hong Chao, Hong Rao, "The study of ssti between guizhou-guangdong ii ±500 kv dc transmission link and steam-turbine-generators near the rectifier termi-

nal," *2006 International Conference on Power System Technology*, 2006. (Accessed 02-05-2023) https://ieeexplore.ieee.org/document/4115898.

[36] Tong Shi, Dulika Nayanasiri, Yunwei (Ryan) Li, "Sub-synchronous oscillations in wind farms – an overview study of mechanisms and damping methods," *IET Renewable Power Generation*, 2021. (Accessed 22-05-2020) https://ietresearch.onlinelibrary.wiley.com/doi/10.1049/iet-rpg.2020.0479.

[37] "INTERCOMPANY REFERENCE 2460288 / 2.0,"

[38] "INTERCOMPANY REFERENCE 1939482 / 4.0,"

[39] Sandra Thengius, "Fault current injection from power electronic interfaced devices," *Kungliga Tekniska Högskolan*, 09 2020. (Accessed 19-01-2023) https://www.svk.se/siteassets/5.jobba-har/dokument-exjobb/fault-current-injection-from-power-electronic-interfaced-devices-2020.pdf.

[40] Ikram Nacef, Khadija Ben Kilani, Mohamed Elleuch, "Understanding inter-area oscillations in power systems integrating wind power," *2018 International Conference on Electrical Sciences and Technologies in Maghreb (CISTEM)*, 10 2018. (Accessed 12-04-2023) https://ieeexplore.ieee.org/stamp/stamp.jsp?tp=&arnumber=8613552.

[41] Nilanjan Ray Chaudhuri et al., "Power oscillation damping control using wide-area signals: A case study on nordic equivalent system," *IEEE PES TD 2010*, 04 2010. (Accessed 12-04-2023) https://ieeexplore.ieee.org/stamp/stamp.jsp?tp=&arnumber=5484295.

[42] Thyge Knüppel et al., "On small-signal stability of wind power system with full-load converter interfaced wind turbines," 2010. (Accessed 17-04-2023) https://backend.orbit.dtu.dk/ws/files/4973185/master.pdf.

[43] Wuhui Chen et al., "Small-signal performance of type 4 wind turbine generator-based clusters in power systems," *Energies*, 06 2018. (Accessed 17-04-2023) https://www.mdpi.com/1996-1073/11/6/1486.

[44] A. Adamczyk, R. Teodorescu, "Control of full-scale converter based wind power plants for damping of low frequency system oscillations," *2011 IEEE Trondheim PowerTech*, 2011. (Accessed 18-04-2023) https://ieeexplore.ieee.org/stamp/stamp.jsp?tp=&arnumber=6019421&tag=1.

[45] Jovana Dakic et al., "Deliverable 2.1 – Work Package 2: Progress report on review and evaluation of OWPP control systems, collection configurations & transmission technologies, offshore electrical resonance instability phenomenon," *INNODC*, 2018. (Accessed 25-05-2023) https://innodc.org/wp-content/uploads/2019/03/Review-and-evaluation-of-OWPP-control-systems-collection-transmission-Aug-2018.pdf.

[46] Mayur Basu et al., "Interarea-oscillation damping with dual power oscillation damping controller of a utility-scale wind power plant," *2021 3rd International Conference on High Voltage Engineering and Power Systems (ICHVEPS)*, 2021. (Accessed 25-05-2023) https://ieeexplore.ieee.org/stamp/stamp.jsp?tp=&arnumber=9601127.

[47] Andrzej Grzegorz Adamczyk et al., "Facts devices for large wind power plants," *Proceedings of the EPE Wind Energy Chapter Symposium 2010*, 2010. (Accessed 16-06-2023) https://vbn.aau.dk/ws/portalfiles/portal/46615856/ANA_EPE2010_FACTS_Devices_for_Large_Wind_Power_Plants.pdf.

[48] Aboutaleb Haddadi et al., "Impact of inverter-based resources on negative sequence quantities-based protection elements," *IEEE TRANSACTIONS ON POWER DELIVERY*, 02 2021. (Acessed 2023-06-13) https://ieeexplore.ieee.org/stamp/stamp.jsp?tp=&arnumber=9022918.

A

Appendix - Unit interference factor with unsaturated subtransient impedance's

Table A.1: UIF for G32 and SCC at the bus closest to the WPP for different models and grid strengths, with unsaturated subtransient impedance's.

Model	Grid strength	SC_{TOT} (MVA)	SC (MVA)	UIF
Standard	High	4124	4091	0.0001
Standard	Low	2648	2395	0.0202
Parallel	High	4508	4439	0.0005
Parallel	Low	2707	2444	0.0210
Own line	High	3639	3585	0.0005
Own line	Low	2379	2167	0.0175

Table A.2: UIF for G42 and SCC at the bus closest to the WPP for different models and grid strengths, with unsaturated subtransient impedance's

Model	Grid strength	SC_{TOT} (MVA)	SC (MVA)	UIF
Standard	High	4124	3916	0.0056
Standard	Low	2898	2395	0.0667
Parallel	High	4508	4361	0.0024
Parallel	Low	2889	2444	0.0527
Own line	High	3639	3572	0.0007
Own line	Low	2449	2167	0.0293

Table A.3: UIF for G42 and SCC at the bus closest to the WPP for different models and grid strengths, in the case of HVDC connection, with unsaturated subtransient impedance's

Model	**Grid strength**	**SC_{TOT} (MVA)**	**SC (MVA)**	**UIF**
Standard	High	5656	5295	0.0092
Standard	Low	3582	2876	0.0873
Parallel	High	6404	6132	0.0041
Parallel	Low	3765	3081	0.0742
Own line	High	4815	4728	0.0007
Own line	Low	3122	2691	0.0429

DEPARTMENT OF SOME SUBJECT OR TECHNOLOGY
CHALMERS UNIVERSITY OF TECHNOLOGY
Gothenburg, Sweden
www.chalmers.se

CHALMERS
UNIVERSITY OF TECHNOLOGY